



HAL
open science

Lysosomal membrane proteins LAMP1 and LIMP2 are segregated in the Golgi apparatus independently of their clathrin adaptor binding motif

Jason Ecard, Yen-Ling Lian, Séverine Divoux, Zelia Gouveia, Emmanuelle Vigne, Franck Perez, Gaelle Boncompain

► To cite this version:

Jason Ecard, Yen-Ling Lian, Séverine Divoux, Zelia Gouveia, Emmanuelle Vigne, et al.. Lysosomal membrane proteins LAMP1 and LIMP2 are segregated in the Golgi apparatus independently of their clathrin adaptor binding motif. *Molecular Biology of the Cell*, 2024, 35 (3), 10.1091/mbc.E23-06-0251 . hal-04736401

HAL Id: hal-04736401

<https://hal.science/hal-04736401v1>

Submitted on 14 Oct 2024

HAL is a multi-disciplinary open access archive for the deposit and dissemination of scientific research documents, whether they are published or not. The documents may come from teaching and research institutions in France or abroad, or from public or private research centers.

L'archive ouverte pluridisciplinaire **HAL**, est destinée au dépôt et à la diffusion de documents scientifiques de niveau recherche, publiés ou non, émanant des établissements d'enseignement et de recherche français ou étrangers, des laboratoires publics ou privés.

1 **Lysosomal membrane proteins LAMP1 and LIMP2 are segregated in the Golgi**
2 **apparatus independently of their clathrin adaptor binding motif.**

3
4
5 Jason Ecard^{1,2}, Yen-Ling Lian¹, Séverine Divoux¹, Zelia Gouveia¹, Emmanuelle
6 Vigne², Franck Perez^{1*} and Gaelle Boncompain^{1*}

7 ¹ Dynamics of Intracellular Organization Laboratory, Institut Curie, PSL Research
8 University, Sorbonne Université, Centre National de la Recherche Scientifique, UMR
9 144, Paris, France.

10 ² Large Molecule Research, Sanofi, Vitry-sur-Seine, France.

11 * contributed equally
12

13 **Abstract**

14 To reach the lysosome, lysosomal membrane proteins (LMPs) are translocated in the
15 endoplasmic reticulum after synthesis and then transported to the Golgi apparatus.
16 The existence of a direct transport from the Golgi apparatus to the endosomes but
17 also of an indirect route through the plasma membrane has been described.
18 Clathrin adaptor binding motifs contained in the cytosolic tail of LMPs have been
19 described as key players in their intracellular trafficking. Here we used the RUSH
20 assay to synchronise the biosynthetic transport of multiple LMPs. After exiting the
21 Golgi apparatus, RUSH-synchronised LAMP1 was addressed to the cell surface both
22 after overexpression or at endogenous level. Its YXXΦ motif was not involved in the
23 transport from the Golgi apparatus to the plasma membrane but in its endocytosis.
24 LAMP1 and LIMP2 were sorted from each other after reaching the Golgi apparatus.
25 LIMP2 was incorporated in punctate structures for export from the Golgi apparatus
26 from which LAMP1 is excluded. LIMP2-containing post-Golgi transport intermediates
27 did not rely neither on its adaptor binding signal nor on its C-terminal cytoplasmic
28 domain.
29

30 **Abbreviations**

31 CLEM: Correlative Light-Electron Microscopy
32 EGFP: Enhanced Green Fluorescent Protein
33 ER: Endoplasmic Reticulum
34 FP: Fluorescent Protein
35 LE/Lys.: Late Endosomes and Lysosomes
36 LMP: Lysosomal Membrane Protein
37 RUSH: Retention Using Selective Hooks
38 SBP: Streptavidin Binding Peptide
39 TGN: *Trans*-Golgi Network
40 TIRF: Total Internal Fluorescence Microscopy
41 MPR: Mannose-6-Phosphate Receptors

43 Introduction

44 Lysosomes are membrane-bound organelles ensuring multiple functions necessary to
45 cellular homeostasis such as degradation of molecules. Lysosomal proteins include
46 soluble luminal enzymes and membrane integral proteins. For their delivery to late
47 endosomes and lysosomes (LE/Lys.), neo-synthesised lysosomal membrane proteins
48 (LMPs) are translocated into the endoplasmic reticulum (ER) and transported to the
49 Golgi apparatus. From there, LMP can follow a direct Golgi-to-endosome transport
50 route, referred to as the direct pathway. Alternatively, they can be targeted to the
51 plasma membrane and reach the endosomes by endocytosis, this pathway being
52 called the indirect pathway (Braulke and Bonifacino, 2009).

53 Lysosomal Integral Membrane Protein 2 (LIMP2) is a type III LMP, which spans the
54 membrane twice. It functions as a receptor for the transport of the lysosomal enzyme
55 β -cerebrosidase to lysosomes (Reczek et al., 2007). In addition, LIMP2 potentially
56 works as a lipid transporter (Conrad et al., 2017; Heybrock et al., 2019; Kuronita et al.,
57 2002). LIMP2 follows a direct pathway to reach LE/Lys after transiting through the
58 Golgi apparatus (Obermuller et al., 2002; Vega et al., 1991). The [D/E]XXXL[L/I] signal
59 (X referring to any amino acid) in its cytoplasmic tail was shown to bind clathrin adaptor
60 complexes AP1, AP2 and AP3, but not AP4, and to be important for its trafficking
61 (Fujita et al., 1999; Honing et al., 1998; Janvier et al., 2003; Le Borgne et al., 1998;
62 Mattera et al., 2011; Ogata and Fukuda, 1994; Sandoval and Bakke, 1994; Sandoval
63 et al., 2000; Tabuchi et al., 2000; Vega et al., 1991). LIMP2-AP1 interaction was
64 proposed to mediate the incorporation of LIMP2 within clathrin-coated vesicles at the
65 *trans*-Golgi Network (TGN) allowing its exit from the Golgi apparatus (Fujita et al.,
66 1999).

67 Lysosomal-Associated Membrane Protein 1 (LAMP1) trafficking pathway is more
68 controversial. Depending on the cell model, LAMP1 was shown to appear at the cell
69 surface during its transport in some studies (Furuno et al., 1989b; Lippincott-Schwartz
70 and Fambrough, 1986; Lippincott-Schwartz and Fambrough, 1987) but not in others
71 (Akasaki et al., 1995; Green et al., 1987). These differences were imputed to variable
72 LAMP1 expression levels. It was proposed that high LAMP1 expression would lead to
73 an overflow of the direct pathway and to its appearance at the cell surface (Harter and
74 Mellman, 1992). LAMP1 bears a GYXX Φ signal (Φ referring to a bulky hydrophobic
75 amino acid) in its cytoplasmic tail, the mutation of which abolishes its trafficking to
76 lysosomes and redirects LAMP1 to the plasma membrane (Guarnieri et al., 1993;
77 Harter and Mellman, 1992; Honing and Hunziker, 1995; Hunziker et al., 1991; Williams
78 and Fukuda, 1990). This signal was shown to bind AP1, AP2 and AP3 (Dell'Angelica
79 et al., 1999; Honing et al., 1996; Le Borgne et al., 1998; Ohno et al., 1996; Ohno et
80 al., 1995). Although AP1 was proposed to participate in the Golgi export of LAMP1
81 (Honing et al., 1996), LAMP1 still reaches lysosomes in AP1-depleted cells (Meyer et
82 al., 2000). LAMP1 has been detected in clathrin-coated pits at the plasma membrane
83 by electron microscopy (Furuno et al., 1989a). Its endocytosis is dependent on
84 clathrin, dynamin and AP2 (Janvier and Bonifacino, 2005). LAMP1 is overexposed at

85 the cell surface in AP3-depleted cells due to an increased recycling, suggesting a role
86 for AP3 in the targeting of LAMP1 from early endosomes to LE/Lys (Dell'Angelica et
87 al., 1999; Peden et al., 2004).

88 Chen *et al.* synchronised the anterograde transport of rat LAMP1 using the Retention
89 Using Selective Hooks (RUSH) system (Chen et al., 2017). Briefly, the tagging of the
90 protein of interest with Streptavidin Binding Peptide (SBP) and the co-expression of
91 an ER-resident streptavidin-tagged protein maintains the protein of interest in the ER
92 until biotin is added to the medium (Boncompain et al., 2012). Chen *et al.* have shown
93 that RUSH-synchronised rat LAMP1 exits the Golgi apparatus in tubulovesicular
94 compartments, which fuse with the plasma membrane. These tubulovesicular
95 compartments also contained plasma membrane-fated proteins, such as the
96 transferrin receptor and VSV-G. In addition, none of the four APs complexes (AP1-4)
97 appeared to be necessary for LAMP1 export from the Golgi apparatus (Chen et al.,
98 2017).

99 Here, we study the trafficking pathway of human LAMP1 using the RUSH system and
100 we demonstrate that RUSH-synchronised LAMP1 follows an indirect pathway to the
101 LE/Lys. independently of its adaptor binding signal. The synchronised transport of
102 other LMPs was analysed and compared to the transport pathway of LAMP1. Our
103 results show that LAMP1 and LIMP2 are segregated and sorted in the Golgi apparatus,
104 LIMP2 being incorporated into punctate structures before being exported from the
105 Golgi apparatus. These LIMP2-containing post-Golgi transport intermediates were
106 shown to be clathrin-free and to rely neither on its adaptor binding signal nor on its C-
107 terminal cytoplasmic domain.

108
109
110

111 Results

112 **Newly synthesised LAMP1 is transported from the Golgi apparatus to the** 113 **plasma membrane before reaching the lysosomes**

114 The anterograde transport of newly synthesised human LAMP1 was analysed using
115 the RUSH system (Boncompain et al., 2012). LAMP1 was fused to a Streptavidin
116 Binding Peptide (SBP) and a fluorescent protein in its luminal domain and transiently
117 expressed in HeLa cells. In the absence of biotin, SBP-mCherry-LAMP1 was retained
118 in the ER thanks to the co-expression of the ER-resident Streptavidin-KDEL (**Fig.**
119 **S1a**). Synchronous release of SBP-mCherry-LAMP1 was induced by addition of biotin.
120 35 min after addition of biotin, SBP-mCherry-LAMP1 was detected in the Golgi
121 apparatus as shown by the colocalisation with the Golgi marker GM130. 2h after
122 addition of biotin, SBP-mCherry-LAMP1 reached the late endosomes/lysosomes
123 (LE/Lys.), as evidenced by the colocalisation with LAMTOR4 (**Fig. S1a,b**). An
124 immunostaining on non-permeabilized cells using an anti-GFP antibody revealed that
125 newly synthesised SBP-EGFP-LAMP1 was detected at the plasma membrane 35 min
126 and 60 min after the addition of biotin (**Fig. 1a**). Flow cytometry was used to monitor

127 the appearance of SBP-EGFP-LAMP1 at the cell surface thanks to immunostaining
128 with an anti-GFP antibody on non-permeabilized cells. The presence of SBP-EGFP-
129 LAMP1 at the cell surface 30 min after its release from the ER was confirmed, peaked
130 after 45 min and then decreased to reach the basal level after 90 min. The basal level
131 of SBP-EGFP-LAMP1 at the cell surface was assessed by the condition in which biotin
132 was added at the time of transfection (no interaction between SBP and Streptavidin
133 occurs) (**Fig. 1b**). The synchronisation of the transport of SBP-EGFP-LAMP1 and its
134 appearance at the cell surface were validated in the breast cancer cell line SUM159
135 and in the non-tumorigenic RPE-1 cell line (**Fig. S1c-e**).

136 To rule out that the appearance of LAMP1 at the cell surface is due to high expression,
137 we engineered the LAMP1 locus using CRISPR/Cas9 to synchronise the anterograde
138 transport of endogenous LAMP1. SUM159 cells were genome-edited to insert SBP
139 and mCherry at the N-terminus of LAMP1 downstream of the signal peptide (**Fig. S2a**).
140 A clonal population with homozygous insertion of SBP-mCherry in LAMP1 gene was
141 then further transduced to express Str-KDEL, necessary for synchronisation of
142 transport using the RUSH assay (**Fig. S2b**). The transport of endogenously tagged
143 LAMP1 (SBP-mCherry-LAMP1^{EN}) was efficiently synchronised from the ER to the
144 lysosome upon addition of biotin (**Fig. S2c**). SBP-mCherry-LAMP1^{EN} was detected by
145 flow cytometry and immunostaining with an anti-SBP antibody at the cell surface of
146 non-permeabilized cells 30 min after incubation with biotin, provided the ER hook was
147 co-expressed (**Fig. S2d**).

148 Using Total Internal Reflection Fluorescence (TIRF) microscopy, fusion events of
149 SBP-EGFP-LAMP1-containing carriers with the plasma membrane were observed
150 (**Fig. 1c, d; Movie 1**). Quickly after fusion has occurred, SBP-EGFP-LAMP1 was
151 trapped in punctate structures, which are positive for mCherry-clathrin Light chain
152 indicating they might be clathrin-coated pits. The signal intensity of SBP-EGFP-
153 LAMP1 in clathrin-coated pits then decreased suggesting its internalisation through
154 endocytosis. TIRF microscopy also showed that carriers containing LAMP1 and fusing
155 with the plasma membrane were positive for RAB6 (**Fig. 1 e-g; Movie 2**). RAB6 is a
156 Ras-related small GTPase involved in the regulation of trafficking pathways from the
157 Golgi apparatus (Fourriere et al., 2019; Girod et al., 1999; Grigoriev et al., 2007;
158 Grigoriev et al., 2011; Patwardhan et al., 2017; White et al., 1999). Previous studies
159 have shown that RAB6 is a major regulator of the formation of post-Golgi carriers
160 (Miserey-Lenkei et al., 2017; Miserey-Lenkei et al., 2010; Pereira et al., 2023) and
161 their delivery to the exocytic sites (Fourriere et al., 2019; Grigoriev et al., 2011).

162 Taken together, our results demonstrate that newly synthesised human LAMP1 is
163 transported from the Golgi apparatus to the plasma membrane before being
164 internalised via clathrin coated pits and transported to its final endosomal destination,
165 late endosomes and lysosomes.

166 **Golgi-to-plasma membrane transport of LAMP1 is not dependent on its YXXΦ** 167 **motif**

168 The clathrin adaptor complexes AP1, AP2, AP3 and AP4 have been shown to
169 recognise YXXΦ motifs in the cytosolic tail of proteins (Robinson, 2004). The motif

170 ⁴¹⁴YQTI₄₁₇ of LAMP1 (**Fig. 3a**) was suggested to be involved in its direct Golgi-to-
171 endosome transport pathway (Cook et al., 2004; Honing et al., 1996; Obermuller et
172 al., 2002). We mutated the LAMP1 critical tyrosine residue Tyr₄₁₄ to Alanine (Y414A).
173 2 h after release from the ER, RUSH-synchronised LAMP1^{Y414A} was localised at the
174 plasma membrane whereas LAMP1 wild-type reached LE/Lys. (**Fig. 2a; Movie 3**). No
175 fluorescent signal of LAMP1^{Y414A} was detected in intracellular compartments. The
176 appearance and persistence of SBP-EGFP-LAMP1^{Y414A} at the cell surface was
177 confirmed by flow cytometry using anti-GFP immunostaining on non-permeabilized
178 cells (**Fig. 2b**). Interestingly, LAMP1^{Y414A} and wild-type LAMP1 were not sorted at the
179 Golgi apparatus and exited from the Golgi apparatus in the same tubulovesicular
180 intermediates (**Fig. 2c, d; Movie 4**). TIRF microscopy showed that LAMP1 wild-type
181 and LAMP1^{Y414A} containing carriers fused with the plasma membrane in the same
182 exocytic events indicating that LAMP1 wild-type and LAMP1^{Y414A} have not been sorted
183 after Golgi exit (**Fig. 2e-g; Movie 5**). Consistent with the role of ⁴¹⁴YQTI₄₁₇ motif in the
184 recruitment of AP2 at clathrin-coated pits, SBP-mCherry-LAMP1^{Y414A} was not enriched
185 in punctate structures at the plasma membrane but diffused quickly in the plasma
186 membrane (**Fig. 2e-g**).
187 These results show that LAMP1 wild-type and LAMP1^{Y414A} follow the same Golgi-to-
188 plasma membrane transport route. The presence of LAMP1^{Y414A} at the plasma
189 membrane exclusively and the absence of sorting of LAMP1 wild-type and LAMP1^{Y414A}
190 at the Golgi apparatus argue against the existence of a direct Golgi-to-endosome
191 transport route.

192 **LAMP1 and LIMP2 are sorted at the Golgi apparatus.**

193 The anterograde transport of several lysosomal membrane proteins (LMPs) was then
194 analysed using the RUSH assay and compared to the trafficking of LAMP1.
195 In addition to LAMP1, LIMP2, LAMP2 and Lysosomal Acid Phosphatase (LAP) were
196 used as RUSH cargos. LAMP2 and Lysosomal Acid Phosphatase (LAP) are type I
197 LMPs. LAP is a luminal lysosomal enzyme, synthesised as a membrane bound
198 protein. The luminal domain, which bears its enzymatic activity, is cleaved upon
199 reaching LE/Lys. (Braun et al., 1989; Waheed et al., 1988). LAMP2, LAP and LIMP2
200 were retained in the ER in the absence of biotin thanks to the co-expression of an ER-
201 resident hook (**Fig. S3**). After the addition of biotin, RUSH-synchronised LAMP2, LAP
202 and LIMP2 were detected in the Golgi apparatus. 2 h after their release from the ER,
203 they reached LE/Lys. as confirmed by immunostaining of LAMTOR4 (**Fig. S3**). The
204 distribution of these proteins at the Golgi apparatus was observed with a higher
205 resolution using a Live-SR module (from Gataca Systems). This system is based on
206 an optically demodulated structure illumination technique and increases the resolution
207 by a factor ≈ 2 , leading to a maximum xy resolution of ≈ 120 -140 nm at the used
208 acquisition setting (Azuma and Kei, 2015). High-resolution images showed that both
209 LAMP2 and LAP were fully colocalized with LAMP1 in the Golgi apparatus (**Fig. S4a,**
210 **b and Fig. S5a, b**). In addition, time-lapse microscopy showed that LAMP2 and LAP
211 exited the Golgi apparatus in the same tubulovesicular carriers as LAMP1 (**Fig. S4c,**
212 **d and Fig S5c, d; Movie 6 and Movie 7**), indicating that no sorting of these LMPs

213 occurred at the Golgi apparatus. LAMP2 and LAP were transiently detected at the cell
214 surface by flow cytometry after their synchronous release from the ER (**Fig. S4e and**
215 **S5e**) as previously shown for LAMP1 (**Fig. 1b**). Interestingly, RUSH-synchronised
216 LIMP2 was segregated from LAMP1 at the Golgi apparatus as highlighted by high-
217 resolution microscopy. In addition to a diffuse localisation in the Golgi apparatus,
218 similar to LAMP1, LIMP2 was detected in puncta with higher fluorescence intensity
219 (**Fig. 3b, c**). Segregation of LIMP2 and LAMP1 in the Golgi apparatus was also
220 detected in SUM159 and RPE-1 cells (**Fig. S6**). Time-lapse imaging showed that
221 LIMP2 was first diffusely localised at the Golgi apparatus and then enriched in bright
222 puncta (**Fig. 3d, e; Movie 8**). After appearance, these puncta remained associated
223 with the Golgi apparatus for several minutes before leaving it (**Fig. 3d, e**). LAMP1-
224 containing tubulovesicular carriers and LIMP2-containing vesicular carriers were
225 distinct and described spatially independent Golgi exit routes (**Fig. 3f; Movie 8**). Cryo-
226 immuno electron microscopy experiments showed that, 25 min after biotin addition,
227 LAMP1 was distributed in several cisternae of the Golgi stack whereas LIMP2 was
228 segregated in small vesicles apposed to the Golgi cisternae, confirming the
229 segregation between LAMP1 and LIMP2 (**Fig. 3h**). Those LIMP2-positive vesicles
230 appeared to be non-coated and LIMP2 was absent from visible peri-Golgi clathrin-
231 coated vesicles (**Fig. 3h**). We also performed correlative light-electron microscopy
232 (CLEM) experiments, which showed that whereas SBP-mCherry-LAMP1 fluorescence
233 overlaps the entire Golgi stack, SBP-EGFP-LIMP2 bright puncta were localised in
234 regions rich in vesicles with a diameter of 50-70 nm (**Fig. 3i-k**).

235

236 Our data demonstrated that LAMP1, LAMP2 and LAP are not sorted and follow the
237 same transport pathway to the plasma membrane. In contrast, LAMP1 and LIMP2 are
238 segregated at the level of the Golgi complex and leave it in morphologically different
239 carriers.

240

241 **The di-Leucine-like motif of LIMP2 is not involved in its export from the Golgi** 242 **apparatus**

243 LIMP2 has been suggested to follow a direct Golgi-to-endosome transport pathway
244 (Obermuller et al., 2002; Vega et al., 1991) depending on its di-leucine-like motif
245 ([D/E]XXXL[L/I]) (Ogata and Fukuda, 1994), which is involved in binding to AP3 and
246 in its transport to lysosomes (Honing et al., 1998; Le Borgne et al., 1998). The critical
247 Leucine 475 and Isoleucine 476 residues (**Fig. 3a**) of LIMP2 were mutated to Alanine,
248 mutant hereafter named LIMP2^{AA}. At steady state, SBP-mApple-LIMP2^{AA} displayed
249 an increased presence at the plasma membrane compared to wild-type LIMP2 (**Fig.**
250 **4a**). However, LIMP2^{AA} reached the same final intracellular compartments as wild-type
251 LIMP2 as highlighted by the condition in which biotin was added at the time of
252 transfection (**Fig. 4a**). The mutation of the [D/E]XXXL[L/I] motif of LIMP2 did not
253 prevent the formation of LIMP2 bright puncta at the Golgi apparatus, LIMP2^{AA} and
254 wild-type LIMP2 being enriched in the same puncta (**Fig. 4b**). LIMP2^{AA} and wild-type
255 LIMP2 left the Golgi apparatus in the same post-Golgi transport intermediates (**Fig.**
256 **4c, d; Movie 9**). LIMP2 was shown to be able to dimerise (Conrad et al., 2017). When

257 expressed alone, LIMP2^{AA} and wild-type LIMP2 displayed the same localisation as
258 when being co-expressed, ruling out that interaction between the wild-type and the
259 mutant forms of LIMP2 would affect their respective transport route. At steady state,
260 LIMP2^{AA} was present at the plasma membrane and at LE/Lys. whereas wild-type
261 LIMP2 was detected at LE/Lys. only (**Fig. S7a, b**). At the Golgi apparatus, LIMP2^{AA}
262 expressed alone behaved similarly to wild-type LIMP2, with the appearance of bright
263 puncta (**Fig S7c, d**). Finally, using high-resolution fluorescence microscopy we
264 showed that LIMP2-containing bright puncta did not colocalize with exogenously
265 expressed mCherry-clathrin light chain (**Fig. 4e-g**).
266 In conclusion, the clathrin adaptor binding motif [D/E]XXXL[L/I] of LIMP2 is not
267 involved in the segregation of LIMP2 at the Golgi apparatus nor in its export from the
268 Golgi apparatus.

269 **LIMP2 C-terminal cytosolic domain is not involved in its segregation at the** 270 **Golgi apparatus**

271 We next investigated whether LIMP2 export from the Golgi might depend on another
272 yet unidentified cytosolic signal. As a type III protein, LIMP2 spans the membrane
273 twice and has two cytosolic domains. Its N-terminal cytosolic domain comprises only
274 4 residues, including the initiating methionine residue (**Fig. 3a**). We therefore focused
275 on its C-terminal cytosolic domain. Domain swapping experiments between LAMP1
276 and LIMP2 cytosolic domains were conducted. RUSH chimeras where the LAMP1
277 cytosolic domain was replaced with the LIMP2 C-terminal cytosolic domain
278 (LAMP1^{LIMP2C}) and the LIMP2 C-terminal cytosolic domain replaced by the LAMP1
279 cytosolic domain (LIMP2^{LAMP1C}) were generated (**Fig. 5a**). A deletion mutant of LIMP2
280 missing the whole C-terminal cytosolic domain was also generated (LIMP2^{ΔC}). Among
281 these constructs, only RUSH-synchronised LIMP2^{LAMP1C} and LIMP2^{ΔC} displayed a
282 punctate localization at the Golgi in contrast to LAMP1^{LIMP2C} (**Fig. 5b**). In conclusion,
283 LIMP2 C-terminal cytosolic domain is neither sufficient nor necessary to induce the
284 enrichment of LMPs in these punctate structures at the Golgi apparatus.
285

286 **Discussion**

287 Our study demonstrates that human LAMP1 reaches the LE/Lys after transiting
288 through the plasma membrane, thus following an indirect pathway from the
289 endoplasmic reticulum to the lysosome. This trafficking route is observed in cells
290 overexpressing RUSH-synchronised LAMP1 as well as at endogenous expression
291 level when the LAMP1 gene is tagged with RUSH-compatible domains. This suggests
292 that the secretory compartments are not overloaded due to high expression,
293 contradicting previous hypotheses (Harter and Mellman, 1992). Mutating LAMP1
294 YXXΦ cytosolic signal does not change the nature of its post-Golgi carriers, indicating
295 that this motif is not involved in sorting at the level of the Golgi apparatus. Our present
296 data confirm previous results from Chen *et al.* who used RUSH-synchronised rat
297 LAMP1 and LAMP1^{Y404A} (Chen *et al.*, 2017). We show that RUSH-synchronised
298 human wild-type LAMP1 and LAMP1^{Y414A} were fully colocalised in post-Golgi transport

299 intermediates. Chen *et al.* showed that LAMP1^{Y404A} was addressed from the Golgi
300 apparatus to the plasma membrane in tubulovesicular carriers as rat wild-type LAMP1
301 does. This rules out the existence of a direct transport pathway from the ER to the
302 LE/Lys for LAMP1 dependent on its APs binding signal, at least in our experimental
303 conditions or if it does exist, the direct transport is very minor. Pols *et al.* have shown
304 that LAMP1 and LAMP2 localise in post-Golgi uncoated compartments devoid of
305 cation-independent mannose-6-phosphate receptor (CI-MPR) in several cell lines,
306 including HeLa cells (Pols *et al.*, 2013). These structures were positive for the
307 CORVET/HOPS subunit Vps41 as well as for the SNARE VAMP7 and were proposed
308 to mediate direct trafficking to endosomes (Pols *et al.*, 2013). However, we and others
309 (Chen *et al.*, 2017) did not detect such a pathway using the synchronisation of the
310 biosynthetic transport of lysosomal membrane, suggesting that either this pathway is
311 insignificant, or that the tagging with SBP prevents its manifestation.

312 LAMP1 endocytosis and targeting to lysosomes have been shown to be dependent on
313 clathrin and AP2 (Chen *et al.*, 2017; Furuno *et al.*, 1989a; Janvier and Bonifacino,
314 2005). We showed that when reaching the plasma membrane, LAMP1 is quickly
315 trapped in clathrin-positive areas. The incorporation of LAMP1 in clathrin-coated
316 structures is dependent on its YXXΦ motif. This process is highly dynamic and
317 efficient, explaining why it is difficult to detect endogenous LAMP1 at the cell surface
318 at steady state.

319 Our data showed that LAMP1, LAMP2 and LAP follow the same transport route from
320 the Golgi apparatus to lysosomes via the plasma membrane, in accordance with
321 previous studies (Braun *et al.*, 1989; Nabi *et al.*, 1991; Obermuller *et al.*, 2002).

322 As LIMP2 was proposed to follow a direct pathway from the Golgi apparatus to
323 endosomes (Obermuller *et al.*, 2002; Vega *et al.*, 1991), one could expect LIMP2 to
324 be sorted from LAMP1/LAMP2/LAP at the Golgi apparatus. Consistently, although
325 LAMP1 and LIMP2 were colocalised when they reach the Golgi apparatus, LIMP2 then
326 concentrated in punctate structures from which LAMP1 was absent. This result
327 demonstrated that segregation occurs at the level of the Golgi apparatus. Chen *et al.*
328 have shown sorting of RUSH-synchronised LAMP1 and cation-dependent (CD)-MPR
329 within the Golgi apparatus (Chen *et al.*, 2017). Our results suggest that CD-MPR and
330 LIMP2 do not follow the same pathways. Indeed, LIMP2 post-Golgi transport
331 intermediates were not colocalised with exogenously expressed mCherry-clathrin light
332 chain while Mannose-6-phosphate receptors (MPRs) recruit clathrin through binding
333 to Golgi-localised Gamma ear-containing, Arf-binding adaptors (GGAs) for their exit
334 from the Golgi apparatus (Chen *et al.*, 2017; Doray *et al.*, 2002a; Puertollano *et al.*,
335 2001; Zhu *et al.*, 2001).

336 Both LAMP1 and LIMP2 recruit AP1 via their cytosolic signals *in vitro* (Fujita *et al.*,
337 1999; Honing *et al.*, 1996). LAMP1 has been shown to be present in clathrin-coated
338 vesicles in close proximity of the Golgi apparatus (Honing *et al.*, 1996). However, the
339 depletion of AP1 does not prevent LAMP1 from reaching LE/Lys. (Chen *et al.*, 2017;
340 Janvier and Bonifacino, 2005; Meyer *et al.*, 2000). Here, we show that mutating their
341 APs binding signal does not modify LAMP1 and LIMP2 export from Golgi. In this
342 context, one could wonder whether AP1 is involved in the Golgi exit of these proteins.

343 AP1 also interacts with MPRs and has been proposed to be involved in their export
344 from the Golgi apparatus (Doray et al., 2002b; Ghosh and Kornfeld, 2003; Ghosh and
345 Kornfeld, 2004; Honing et al., 1997; Stockli et al., 2004). However, AP1 depletion or
346 knock-sideway (i.e. docking AP1 on mitochondria membranes) does not result in a
347 blockage of MPRs at the Golgi apparatus, but rather in an enrichment of MPRs in
348 endosomes (Meyer et al., 2000; Robinson et al., 2010). This raises the hypothesis that
349 AP1 could be involved in the retrograde endosome-to-Golgi pathway (Meyer et al.,
350 2000; Robinson et al., 2010). Whether AP1 could have such a role for LAMP1 or
351 LIMP2 is an intriguing question, which deserves further investigation. This could bring
352 an explanation for the presence of LAMP1 in compartments positive for Vps41 and
353 VAMP7 near the Golgi apparatus, as observed by Pols *et al.* (Pols et al., 2013).

354 At steady state (one day after transfection and continuous incubation with biotin), SBP-
355 mApple-LIMP2^{AA} localises in LE/Lys., as does wild-type LIMP2, but also shows an
356 increased presence at the cell surface (**Fig. 4a** and **Fig. S7a-b**). This could be due to
357 impaired endocytosis secondary to LIMP2^{AA} inability to recruit the endocytic
358 machinery. LIMP2 would reach the plasma membrane after exiting the Golgi
359 apparatus, even though an indirect pathway to LE/Lys for LIMP2 is in contradiction
360 with previous published data (Obermuller et al., 2002; Vega et al., 1991), or because
361 of LE/Lys fusion with the plasma membrane. These kinds of fusion events have been
362 described in a multitude of contexts, such as exosome secretion (Kowal et al., 2014),
363 plasma membrane repair (Jimenez and Perez, 2017) or unconventional secretion
364 (Rabouille, 2017). Another possibility would be that LIMP2^{AA} would struggle to
365 orientate to LE/Lys after reaching endosomes, due to its inability to recruit AP3.
366 Increased surface expression of other LMPs such as LAMP1, LAMP2 and CD63 has
367 been described when AP3 is defective (Dell'Angelica et al., 1999). Unfortunately, our
368 results do not allow to conclude on the transport route of LIMP2 to LE/Lys. after its
369 Golgi exit.

370 Post-Golgi transport intermediates containing LIMP2 colocalised with vesicular
371 regions close to the Golgi apparatus, as suggested by our immuno EM and CLEM
372 experiments, but are devoid of clathrin. The mechanisms involved in LIMP2
373 concentration and in the formation of these intermediates require further investigation.
374 Interestingly, LIMP2-containing puncta remain associated with the Golgi apparatus for
375 several minutes before leaving, which could indicate maturation processes might be
376 required for their Golgi exit. As the mutation in the adaptor-binding signal in LIMP2 did
377 not modify its exit from the Golgi apparatus, we investigated whether another motif in
378 its C-terminal cytoplasmic domain could be involved in the formation of LIMP2 post-
379 Golgi transport intermediates. However, the C-terminal cytoplasmic domain of LIMP2
380 appeared neither sufficient nor essential for the formation of LIMP2 bright puncta and
381 its segregation from LAMP1.

382 The contribution of LIMP2's biophysical properties and interactions with partners to the
383 formation of these puncta remains unclear. LIMP2 has been shown to be able to
384 dimerize, allowing it to function as a lipid channel (Conrad et al., 2017; Heybrock et
385 al., 2019). The potential role of the dimerization or the lipid-association of LIMP2 in
386 LIMP2 packing within vesicles at the Golgi apparatus remains open. The lysosomal

387 enzyme beta-glucocerebrosidase (β GC) binds LIMP2 in the ER and uses LIMP2 as a
388 sorting receptor for its transport to lysosomes (Reczek et al., 2007). Deletion or
389 mutations of the β GC-binding region in LIMP2 (luminal residues V149-Y163) did not
390 prevent LIMP2 to reach lysosomes (Blanz et al., 2010; Neculai et al., 2013; Reczek et
391 al., 2007). The 3D conformation of this region has also been shown to be pH-sensitive,
392 allowing the release of β GC in the lumen of lysosomes (Neculai et al., 2013; Reczek
393 et al., 2007; Zachos et al., 2012). Mutations of these pH-sensitive luminal residues
394 (H₁₅₀ and H₁₇₁) did not impair LIMP2 targeting to lysosomes (Zachos et al., 2012).
395 Zhao et al. identified a mannose-6-phosphate (M6P) on LIMP2 and described the
396 formation in vitro of a ternary complex β GC-LIMP2-CI-MPR (Zhao et al., 2014).
397 However, the biological relevance of this M6P was disputed (Blanz et al., 2010).
398 Indeed, several studies have suggested that both β GC and LIMP2 reach lysosomes
399 in a M6P/MPRs-independent manner (Aerts et al., 1988; Blanz et al., 2015; Owada
400 and Neufeld, 1982). Consistently, we showed by immunofluorescence and electron
401 microscopy that RUSH-synchronized LIMP2-containing vesicles lack clathrin, which
402 could confirm that LIMP2 trafficking is unlikely to be MPR-dependent.
403 In depth investigation of the molecular players and intrinsic biophysical properties
404 regulating the transport of LIMP2 in a biological context is needed and extends beyond
405 the scope of our study.

406
407
408

409 **Materials and Methods**

410 **Immunofluorescence and flow cytometry**

411 Cell fixation was performed by incubation in 3% paraformaldehyde (Electron
412 Microscopy Sciences; cat. no. 15710) for 10 min and permeabilised by incubation in
413 0.5 g/L saponin in PBS supplemented with 2 g/L bovine serum albumin. Primary
414 antibodies used in this study were anti-GM130 (BD Transduction Laboratories; cat.
415 no. 610823; dilution 1:1000), anti-giantin (clone TA10; recombinant antibody facility of
416 Institut Curie, Paris, France), anti-LAMTOR4 (Cell Signaling Technology; cat. no.
417 13140 dilution 1:1000), anti-PDI isoform A3 (Sigma-Aldrich; cat. no. AMAB90988;
418 1:250). Fluorochrome conjugated secondary antibodies were purchased from Jackson
419 ImmunoResearch. Coverslips were mounted in Mowiol containing DAPI. In **Fig. S7**,
420 cells were stained with HCS CellMask Blue Stain (ThermoFisher Scientific; cat. no.
421 H32720; diluted at 1:5000 in the mounting medium). For cell surface staining, cells
422 were transferred in ice-cold PBS and incubated with an Alexa Fluor® 647-coupled
423 anti-GFP antibody (BD Pharmingen; cat. no. 565197; dilution 1:150), for 40 min prior
424 to fixation with 2% paraformaldehyde. Signal intensity was analysed by flow cytometry
425 using a BD Accuri™ C6 or a Miltenyi MACSQuant10 cytometer. Median anti-GFP
426 intensity of GFP-positive cells normalised to the maximum value is depicted on the
427 graph.

428
429

429 **Cryo-immuno-electron microscopy**

430 Cells were fixed with 2% paraformaldehyde and 0.2% glutaraldehyde in 0.1M sodium
431 phosphate buffer, pH 7.4. After washing in PBS/Glycine 0,02M, cells were pelleted by
432 centrifugation, embedded in 12% gelatin, cooled in ice and cut into 5-mm³ blocks. The
433 blocks were infused overnight with 2.3 M sucrose at 4°C, frozen in liquid nitrogen and
434 stored until cryo-ultramicrotomy. Sections of 80 nm were cut with a diamond knife
435 (Diatome) at -112°C using Leica EM-UC7. Ultrathin sections were picked up in a mix
436 of 1.8% methylcellulose and 2.3 M sucrose (1:1) according to (Liou et al., 1996) and
437 transferred to formvar carbon-coated copper grids. Double immunolabeling was
438 performed as described before (Slot et al., 1991) with optimal combination of gold
439 particle sizes and sequence of antibodies. Cryosections were first incubated with
440 rabbit polyclonal anti-GFP antibody (invitrogen) followed by protein A gold-15nm (Slot
441 and Geuze, 1985). After post-fixation with 1% glutaraldehyde in PBS, cryosections
442 were incubated with a rabbit polyclonal anti-mCherry antibody (antibody facility of the
443 Institut Curie) followed by protein A gold-10nm. After labelling, the sections were
444 treated with 1% glutaraldehyde, counterstained with uranyl acetate, and embedded in
445 methyl cellulose uranylacetate (Slot et al., 1991). Grids were observed on a Tecnai G2
446 spirit (FEI Company) equipped with a 4-k CCD camera (Quemesa, Olympus).
447

448 **Correlative light-electron microscopy**

449 HeLa cells expressing RUSH cargos were live-stained for 1 h with SiR-lysosome
450 (Spirochrome) and SiR-DNA (Spirochrome) at 1 µM each. The cells were then
451 incubated with biotin for 27 min and fixed with 3% paraformaldehyde (Electron
452 Microscopy Sciences; cat. no. 15710) for 10 min. Fluorescence images were then
453 acquired using an Eclipse 80i microscope (Nikon) equipped with a CSU-X1 Yokogawa
454 spinning-disk head and an Ultra897 iXon EMCCD camera (Andor). The cells were
455 then post-fixed with glutaraldehyde 2.5% in cacodylate buffer 0,1 M, pH 7.2 and then
456 with 1% (w/v) OsO₄ supplemented with 1.5% (w/v) potassium ferrocyanide,
457 dehydrated in increasing concentration of ethanol (50%, 70%, 90%, 96%, 100%). Cells
458 were embedded in epon 812 (TAAB Laboratories Equipment) and processed for serial
459 ultrathin sectioning with a Reichert Ultracut S ultramicrotome (Leica). Sections were
460 counter-stained with uranyl acetate and lead citrate, and observed with a Transmission
461 Electron Microscope (TEM; Tecnai G2 Spirit; FEI) equipped with a Quemesa 4k CCD
462 camera (Olympus).
463 Fluorescence and EM images were correlated based on the SiR-lysosome staining
464 and using the eC-CLEM software (Paul-Gilloteaux et al., 2017).

465 **RUSH constructs and other plasmids**

466 All RUSH constructs were expressed using bicistronic plasmids coding for both SBP-
467 FP-tagged LMP and the hook. SBP-FP-LAMP1 (LAMP1 sequence from NM_005561.3
468 generated from cDNA from GE Dharmacon, Clone ID 3872778), its mutants, SBP-FP-
469 LAMP2 (isoform B, nucleotide sequence NM_013995.2, generated from a plasmid
470 kindly given by Y. Baudat, Sanofi R&D Centre, Vitry sur Seine, France) and SBP-FP-
471 LAP (isoform 1, nucleotide sequence NM_001357016.1 generated from a cDNA from

472 GE Dharmacon, Clone ID 30332133) were used with the luminal hook Streptavidin-
473 KDEL (Boncompain *et al.*, 2012). SBP-FP-LIMP2 (isoform 1, nucleotide sequence
474 NM_005506.3, generated from cDNA from GE Dharmacon, Clone ID 3872778) and
475 its mutants were cytosolically tagged and co-expressed with either Streptavidin-HA-
476 Endo-KKXX or Mini-li-streptavidin. Streptavidin-HA-Endo-KKXX consists in the fusion
477 of streptavidin to the HA-tag, the endocytic signal of LAMP1 (AGYQTI) and the COPI
478 recruitment signal of the *Saccharomyces cerevisiae* WBP1 (KKTN). Mini-li-
479 streptavidin is composed of the sequence coding for the 46 first amino acids of human
480 CD74/li upstream of Streptavidin. All plasmids generated for the present study were
481 verified by sequencing. The EGFP-RAB6 plasmid was a gift from Jamie White (White
482 *et al.*, 1999). The mCherry-clathrin light chain plasmid was a gift from Guillaume
483 Montagnac (Gustave Roussy, Villejuif, France).

484 **Cells culture, transfection and RUSH assay**

485 HeLa cells were grown at 37°C with 5% CO₂ in DMEM, high glucose, GlutaMAX
486 (ThermoFischer Scientific) supplemented with 10% FCS (Biosera), 1 mM sodium
487 pyruvate (ThermoFischer Scientific) and 100 U/mL penicillin and streptomycin
488 (ThermoFischer Scientific). SUM159 cells were cultured in Dulbecco's modified
489 Eagle's medium (DMEM)/F-12 GlutaMAX (GIBCO), supplemented with 5% FCS
490 (Biosera), penicillin-streptomycin (500 µg/ml; GIBCO), hydrocortisone (1 µg/ml;
491 Sigma-Aldrich), insulin (5 µg/ml; Sigma-Aldrich), and 10 mM Hepes (GIBCO). RPE-1
492 cells were cultured in Dulbecco's modified Eagle's medium (DMEM)/F-12 GlutaMAX
493 (GIBCO), supplemented with 10% FCS (Biosera), penicillin-streptomycin (500 µg/ml;
494 GIBCO). HeLa cells were transfected 24h before fixation or observation using calcium
495 phosphate method as previously described (Jordan *et al.*, 1996). SUM159 and RPE-
496 1 cells were transfected using JetPrime (Polyplus). To release RUSH cargos, D-biotin
497 (Sigma-Aldrich; cat. no. B4501) was added to the culture medium at a final
498 concentration of 80 µM.

499

500 **Genome editing of LAMP1**

501 The sequence of the gRNA targeting the exon 2 of human LAMP1 was 5'-
502 AACGGGACCGCGTGCATAA-3' downstream of a U6 promoter and upstream of a
503 gRNA scaffold as previously described in (Mali *et al.*, 2013) and has been inserted in
504 a pCRII vector (Thermo Fisher). The gRNA coding plasmid was co-transfected with a
505 plasmid coding for hCas9 (hCas9 was a gift from George Church (Addgene plasmid #
506 41815 ; <http://n2t.net/addgene:41815> ; RRID:Addgene_41815),
507 a plasmid bearing puromycin resistance (pIRES-puromycin from Clontech; to enrich
508 for transfected cells), the donor plasmid. The donor plasmid was constructed by gene
509 synthesis (Geneart, Thermo Fisher) of the left and right homology arms (800 bp each)
510 and insertion between the two arms of the cassette SBP-mCherry. Please note that
511 we reconstructed in the donor plasmid the signal peptide of LAMP1, which is coded
512 by part of the exon1 and exon 2 (see Fig. S2a). SUM159 cells were transfected using
513 JetPrime (Polyplus) following manufacturer's instructions. 24 h post-transfection

514 puromycin at 5µg/ml was added for 1 day only. After expansion, clones were obtained
515 by limiting dilutions.

516 For characterization, the genomic DNA of the clones was extracted (NucleoTissue kit
517 from Macherey-Nagel) from the engineered SBP-mcherry-LAMP1^{EN} knock-in cell
518 lines, and then PCR genotyping was performed to validate the genomic DNA
519 sequences (1kb upstream of gRNA cutting site forward primer 5'-
520 GCACGGATTCCAGTGGTGGCA-3' and 1kb downstream reverse primer 5'-
521 ATGGTTGGTTGACATGCAATGCAAACA-3'). The genomic sequences of the edited
522 allele in the junction of right and left homologous arms were edited as expected. PCR
523 using forward primer 5'-AAAACCCCGTCGCTACTAAAAACAGAA-3', 5'-
524 AATTCCTGCAGGTGGTTCACGTTGACCTTGTGG-3', 5'-
525 aattcctgcaggTGGTTCACGTTGACCTTGTGG-3', and the reverse primer 5'-
526 GGAAAATGTTCATGATGAACAGTGAGG-3' were used to check the insertion of
527 SBP-mCherry. The genomic DNA sequences of SBP-mCherry CRISPR-Cas9 knock-
528 in were coherent with the expected sequence in the gRNA cutting region of LAMP1

529

530

531 **Fluorescence image acquisition and analysis**

532 Widefield microscopy images were acquired using a Leica DM6000 equipped
533 microscope with a CoolSnap HQ2 (Photometrics) CCD camera. Confocal images of
534 fixed cells were acquired with an Eclipse Ti-E microscope (Nikon) equipped with a
535 CSU-X1 Yokogawa spinning-disk head and a Prime 95B sCMOS camera
536 (Photometrics). High-resolution images were acquired with this same set-up
537 complemented with a Live-SR super-resolution module (Gataca Systems) (Roth and
538 Heintzmann, 2016). This device, based on an optically demodulated structure
539 illumination technique, increases the resolution by a factor ≈ 2 , leading to a maximum
540 xy resolution of ≈ 120 nm at 480 nm and ≈ 140 nm at 561 nm (Azuma and Kei, 2015).
541 For time-lapse imaging, cells were transferred in the CO₂-independent Leibovitz's
542 medium (ThermoFischer Scientific) and were acquired at 37°C in a thermostat-
543 controlled chamber. Confocal live-cell images were acquired with an Eclipse 80i
544 microscope (Nikon) equipped with a CSU-X1 Yokogawa spinning-disk head and an
545 Ultra897 iXon EMCCD camera (Andor). TIRF live-cell images were acquired with an
546 Eclipse Ti-E microscope (Nikon) equipped with a TIRF module (Nikon), a 100x CFI
547 Apo TIRF objective and an Evolve EMCCD camera (Photometrics). All acquisitions
548 were driven by the MetaMorph software (Molecular Devices). Pixel intensity linescans,
549 kymographs (Fig. 1g) and temporal projections were performed thanks to Fiji software
550 (Schindelin et al., 2012) built-in functions *Plot Profile*, *Multi Kymograph* and *Temporal-*
551 *Color Code*, respectively.

552

553 **Acknowledgment**

554 The authors acknowledge the Cell and Tissue Imaging Platform (PICT-IBiSA) of
555 Institut Curie - CNRS UMR144 and the Nikon Imaging Centre at Institut Curie-CNRS,
556 members of the national infrastructure France-BioImaging supported by the French

557 National Research Agency (ANR-10-INBS-04) and the recombinant antibody facility,
558 Institut Curie.

559 We also thank Yves Baudat for his input and for providing the plasmid coding for
560 LAMP2B.

561 The work in FP lab work was supported by Labex Cell(n)Scale (ANR-10-LBX-0038
562 part of the IDEX PSL no. ANR-10- IDEX-0001-02, by the ANR grants ANR-22-CE14-
563 0066-01, ANR-20-CE14-0017-02, ANR-19-CE13-0006-03, ANR-19-CE13-0002-03
564 and by the Fondation pour la Recherche Médicale (EQU201903007925). The grant
565 ANR-20-CE13-0012-01 from Agence Nationale de la Recherche has been attributed
566 to GB. FDT201805005670 has been attributed to JE by the Fondation pour la
567 Recherche Médicale. This work was financially supported by SANOFI (Collaboration
568 agreement SANOFI/Institut Curie/UPMC/CNRS). JE was supported by a CIFRE
569 fellowship (N°2015/0313) funded in part by the National Association for Research and
570 Technology (ANRT) on behalf of the French Ministry of Education and Research, and
571 in part by SANOFI. YLL has been granted with ARC DOC4 from the Fondation ARC
572 pour la Recherche sur le Cancer.

573

574 Declaration of interests

575 JE and EV are Sanofi employees and may hold shares and/or stock options in the
576 company.

577

578 Significance Statement

579 • Lysosomal membrane proteins (LMPs) are transported to the lysosome through the
580 Golgi apparatus. Their mode of biosynthetic delivery remains controversial. How LMPs are
581 segregated in the Golgi and which motifs are involved is unknown.

582 • Using synchronization of their transport, the authors showed that LAMP1 transits
583 through the plasma membrane before reaching the lysosome. LAMP1, LAMP2 and LAP
584 are not segregated in the Golgi while LAMP1 and LAMP2 are.

585 • Mutations of their clathrin adaptor binding motifs suggest that they are not involved in
586 the segregation and sorting of these LMPs at the Golgi apparatus.

587

589 **References**

590

591

- 592 Aerts, J.M., J. Heikoop, S. van Weely, W.E. Donker-Koopman, J.A. Barranger, J.M. Tager,
593 and A.W. Schram. 1988. Characterization of glucocerebrosidase in peripheral blood
594 cells and cultured blastoid cells. *Exp Cell Res.* 177:391-398.
- 595 Akasaki, K., A. Michihara, K. Mibuka, Y. Fujiwara, and H. Tsuji. 1995. Biosynthetic transport
596 of a major lysosomal membrane glycoprotein, lamp-1: convergence of biosynthetic
597 and endocytic pathways occurs at three distinctive points. *Exp Cell Res.* 220:464-
598 473.
- 599 Azuma, T., and T. Kei. 2015. Super-resolution spinning-disk confocal microscopy using
600 optical photon reassignment. *Opt Express.* 23:15003-15011.
- 601 Blanz, J., J. Groth, C. Zachos, C. Wehling, P. Saftig, and M. Schwake. 2010. Disease-
602 causing mutations within the lysosomal integral membrane protein type 2 (LIMP-2)
603 reveal the nature of binding to its ligand beta-glucocerebrosidase. *Hum Mol Genet.*
604 19:563-572.
- 605 Blanz, J., F. Zunke, S. Markmann, M. Damme, T. Braulke, P. Saftig, and M. Schwake. 2015.
606 Mannose 6-phosphate-independent Lysosomal Sorting of LIMP-2. *Traffic.* 16:1127-
607 1136.
- 608 Boncompain, G., S. Divoux, N. Gareil, H. de Forges, A. Lescure, L. Latreche, V. Mercanti, F.
609 Jollivet, G. Raposo, and F. Perez. 2012. Synchronization of secretory protein traffic in
610 populations of cells. *Nat Methods.* 9:493-498.
- 611 Braulke, T., and J.S. Bonifacino. 2009. Sorting of lysosomal proteins. *Biochim Biophys Acta.*
612 1793:605-614.
- 613 Braun, M., A. Waheed, and K. von Figura. 1989. Lysosomal acid phosphatase is transported
614 to lysosomes via the cell surface. *EMBO J.* 8:3633-3640.
- 615 Chen, Y., D.C. Gershlick, S.Y. Park, and J.S. Bonifacino. 2017. Segregation in the Golgi
616 complex precedes export of endolysosomal proteins in distinct transport carriers. *J*
617 *Cell Biol.*
- 618 Conrad, K.S., T.W. Cheng, D. Ysselstein, S. Heybrock, L.R. Hoth, B.A. Chrnyk, C.W. Am
619 Ende, D. Krainc, M. Schwake, P. Saftig, S. Liu, X. Qiu, and M.D. Ehlers. 2017.
620 Lysosomal integral membrane protein-2 as a phospholipid receptor revealed by
621 biophysical and cellular studies. *Nat Commun.* 8:1908.
- 622 Cook, N.R., P.E. Row, and H.W. Davidson. 2004. Lysosome associated membrane protein 1
623 (Lamp1) traffics directly from the TGN to early endosomes. *Traffic.* 5:685-699.
- 624 Dell'Angelica, E.C., V. Shotelersuk, R.C. Aguilar, W.A. Gahl, and J.S. Bonifacino. 1999.
625 Altered trafficking of lysosomal proteins in Hermansky-Pudlak syndrome due to
626 mutations in the beta 3A subunit of the AP-3 adaptor. *Mol Cell.* 3:11-21.
- 627 Doray, B., K. Bruns, P. Ghosh, and S. Kornfeld. 2002a. Interaction of the cation-dependent
628 mannose 6-phosphate receptor with GGA proteins. *J Biol Chem.* 277:18477-18482.
- 629 Doray, B., P. Ghosh, J. Griffith, H.J. Geuze, and S. Kornfeld. 2002b. Cooperation of GGAs
630 and AP-1 in packaging MPRs at the trans-Golgi network. *Science.* 297:1700-1703.
- 631 Fourriere, L., A. Kasri, N. Gareil, S. Bardin, H. Bousquet, D. Pereira, F. Perez, B. Goud, G.
632 Boncompain, and S. Miserey-Lenkei. 2019. RAB6 and microtubules restrict protein
633 secretion to focal adhesions. *J Cell Biol.* 218:2215-2231.
- 634 Fujita, H., M. Saeki, K. Yasunaga, T. Ueda, T. Imoto, and M. Himeno. 1999. In vitro binding
635 study of adaptor protein complex (AP-1) to lysosomal targeting motif (LI-motif).
636 *Biochem Biophys Res Commun.* 255:54-58.
- 637 Furuno, K., T. Ishikawa, K. Akasaki, S. Yano, Y. Tanaka, Y. Yamaguchi, H. Tsuji, M.
638 Himeno, and K. Kato. 1989a. Morphological localization of a major lysosomal

639 membrane glycoprotein in the endocytic membrane system. *J Biochem.* 106:708-
640 716.

641 Furuno, K., S. Yano, K. Akasaki, Y. Tanaka, Y. Yamaguchi, H. Tsuji, M. Himeno, and K.
642 Kato. 1989b. Biochemical analysis of the movement of a major lysosomal membrane
643 glycoprotein in the endocytic membrane system. *J Biochem.* 106:717-722.

644 Ghosh, P., and S. Kornfeld. 2003. AP-1 binding to sorting signals and release from clathrin-
645 coated vesicles is regulated by phosphorylation. *J Cell Biol.* 160:699-708.

646 Ghosh, P., and S. Kornfeld. 2004. The cytoplasmic tail of the cation-independent mannose
647 6-phosphate receptor contains four binding sites for AP-1. *Arch Biochem Biophys.*
648 426:225-230.

649 Girod, A., B. Storrie, J.C. Simpson, L. Johannes, B. Goud, L.M. Roberts, J.M. Lord, T.
650 Nilsson, and R. Pepperkok. 1999. Evidence for a COP-I-independent transport route
651 from the Golgi complex to the endoplasmic reticulum. *Nat Cell Biol.* 1:423-430.

652 Green, S.A., K.P. Zimmer, G. Griffiths, and I. Mellman. 1987. Kinetics of intracellular
653 transport and sorting of lysosomal membrane and plasma membrane proteins. *J Cell*
654 *Biol.* 105:1227-1240.

655 Grigoriev, I., D. Splinter, N. Keijzer, P.S. Wulf, J. Demmers, T. Ohtsuka, M. Modesti, I.V.
656 Maly, F. Grosveld, C.C. Hoogenraad, and A. Akhmanova. 2007. Rab6 regulates
657 transport and targeting of exocytotic carriers. *Dev Cell.* 13:305-314.

658 Grigoriev, I., K.L. Yu, E. Martinez-Sanchez, A. Serra-Marques, I. Smal, E. Meijering, J.
659 Demmers, J. Peranen, R.J. Pasterkamp, P. van der Sluijs, C.C. Hoogenraad, and A.
660 Akhmanova. 2011. Rab6, Rab8, and MICAL3 cooperate in controlling docking and
661 fusion of exocytotic carriers. *Curr Biol.* 21:967-974.

662 Guarnieri, F.G., L.M. Arterburn, M.B. Penno, Y. Cha, and J.T. August. 1993. The motif Tyr-
663 X-X-hydrophobic residue mediates lysosomal membrane targeting of lysosome-
664 associated membrane protein 1. *J Biol Chem.* 268:1941-1946.

665 Harter, C., and I. Mellman. 1992. Transport of the lysosomal membrane glycoprotein Igp120
666 (Igp-A) to lysosomes does not require appearance on the plasma membrane. *J Cell*
667 *Biol.* 117:311-325.

668 Heybrock, S., K. Kanerva, Y. Meng, C. Ing, A. Liang, Z.J. Xiong, X. Weng, Y. Ah Kim, R.
669 Collins, W. Trimble, R. Pomes, G.G. Prive, W. Annaert, M. Schwake, J. Heeren, R.
670 Lullmann-Rauch, S. Grinstein, E. Ikonen, P. Saftig, and D. Neculai. 2019. Lysosomal
671 integral membrane protein-2 (LIMP-2/SCARB2) is involved in lysosomal cholesterol
672 export. *Nat Commun.* 10:3521.

673 Honing, S., J. Griffith, H.J. Geuze, and W. Hunziker. 1996. The tyrosine-based lysosomal
674 targeting signal in lamp-1 mediates sorting into Golgi-derived clathrin-coated
675 vesicles. *EMBO J.* 15:5230-5239.

676 Honing, S., and W. Hunziker. 1995. Cytoplasmic determinants involved in direct lysosomal
677 sorting, endocytosis, and basolateral targeting of rat Igp120 (lamp-I) in MDCK cells. *J*
678 *Cell Biol.* 128:321-332.

679 Honing, S., I.V. Sandoval, and K. von Figura. 1998. A di-leucine-based motif in the
680 cytoplasmic tail of LIMP-II and tyrosinase mediates selective binding of AP-3. *EMBO*
681 *J.* 17:1304-1314.

682 Honing, S., M. Sosa, A. Hille-Rehfeld, and K. von Figura. 1997. The 46-kDa mannose 6-
683 phosphate receptor contains multiple binding sites for clathrin adaptors. *J Biol Chem.*
684 272:19884-19890.

685 Hunziker, W., C. Harter, K. Matter, and I. Mellman. 1991. Basolateral sorting in MDCK cells
686 requires a distinct cytoplasmic domain determinant. *Cell.* 66:907-920.

687 Janvier, K., and J.S. Bonifacino. 2005. Role of the endocytic machinery in the sorting of
688 lysosome-associated membrane proteins. *Mol Biol Cell.* 16:4231-4242.

689 Janvier, K., Y. Kato, M. Boehm, J.R. Rose, J.A. Martina, B.Y. Kim, S. Venkatesan, and J.S.
690 Bonifacino. 2003. Recognition of dileucine-based sorting signals from HIV-1 Nef and
691 LIMP-II by the AP-1 gamma-sigma1 and AP-3 delta-sigma3 hemicomplexes. *J Cell*
692 *Biol.* 163:1281-1290.

693 Jimenez, A.J., and F. Perez. 2017. Plasma membrane repair: the adaptable cell life-
694 insurance. *Curr Opin Cell Biol.* 47:99-107.

695 Jordan, M., A. Schallhorn, and F.M. Wurm. 1996. Transfecting mammalian cells:
696 optimization of critical parameters affecting calcium-phosphate precipitate formation.
697 *Nucleic Acids Res.* 24:596-601.

698 Kowal, J., M. Tkach, and C. Thery. 2014. Biogenesis and secretion of exosomes. *Curr Opin*
699 *Cell Biol.* 29:116-125.

700 Kuronita, T., E.L. Eskelinen, H. Fujita, P. Saftig, M. Himeno, and Y. Tanaka. 2002. A role for
701 the lysosomal membrane protein LGP85 in the biogenesis and maintenance of
702 endosomal and lysosomal morphology. *J Cell Sci.* 115:4117-4131.

703 Le Borgne, R., A. Alconada, U. Bauer, and B. Hoflack. 1998. The mammalian AP-3 adaptor-
704 like complex mediates the intracellular transport of lysosomal membrane
705 glycoproteins. *J Biol Chem.* 273:29451-29461.

706 Liou, W., H.J. Geuze, and J.W. Slot. 1996. Improving structural integrity of cryosections for
707 immunogold labeling. *Histochem Cell Biol.* 106:41-58.

708 Lippincott-Schwartz, J., and D.M. Fambrough. 1986. Lysosomal membrane dynamics:
709 structure and interorganellar movement of a major lysosomal membrane
710 glycoprotein. *J Cell Biol.* 102:1593-1605.

711 Lippincott-Schwartz, J., and D.M. Fambrough. 1987. Cycling of the integral membrane
712 glycoprotein, LEP100, between plasma membrane and lysosomes: kinetic and
713 morphological analysis. *Cell.* 49:669-677.

714 Mali, P., L. Yang, K.M. Esvelt, J. Aach, M. Guell, J.E. DiCarlo, J.E. Norville, and G.M.
715 Church. 2013. RNA-guided human genome engineering via Cas9. *Science.* 339:823-
716 826.

717 Mattera, R., M. Boehm, R. Chaudhuri, Y. Prabhu, and J.S. Bonifacino. 2011. Conservation
718 and diversification of dileucine signal recognition by adaptor protein (AP) complex
719 variants. *J Biol Chem.* 286:2022-2030.

720 Meyer, C., D. Zizioli, S. Lausmann, E.L. Eskelinen, J. Hamann, P. Saftig, K. von Figura, and
721 P. Schu. 2000. mu1A-adaptin-deficient mice: lethality, loss of AP-1 binding and
722 rerouting of mannose 6-phosphate receptors. *EMBO J.* 19:2193-2203.

723 Miserey-Lenkei, S., H. Bousquet, O. Pylypenko, S. Bardin, A. Dimitrov, G. Bressanelli, R.
724 Bonifay, V. Fraisier, C. Guillou, C. Bougeret, A. Houdusse, A. Echard, and B. Goud.
725 2017. Coupling fission and exit of RAB6 vesicles at Golgi hotspots through kinesin-
726 myosin interactions. *Nat Commun.* 8:1254.

727 Miserey-Lenkei, S., G. Chalancon, S. Bardin, E. Formstecher, B. Goud, and A. Echard.
728 2010. Rab and actomyosin-dependent fission of transport vesicles at the Golgi
729 complex. *Nat Cell Biol.* 12:645-654.

730 Nabi, I.R., A. Le Bivic, D. Fambrough, and E. Rodriguez-Boulant. 1991. An endogenous
731 MDCK lysosomal membrane glycoprotein is targeted basolaterally before delivery to
732 lysosomes. *J Cell Biol.* 115:1573-1584.

733 Neculai, D., M. Schwake, M. Ravichandran, F. Zunke, R.F. Collins, J. Peters, M. Neculai, J.
734 Plumb, P. Loppnau, J.C. Pizarro, A. Seitova, W.S. Trimble, P. Saftig, S. Grinstein,
735 and S. Dhe-Paganon. 2013. Structure of LIMP-2 provides functional insights with
736 implications for SR-BI and CD36. *Nature.* 504:172-176.

737 Obermuller, S., C. Kiecke, K. von Figura, and S. Honing. 2002. The tyrosine motifs of Lamp
738 1 and LAP determine their direct and indirect targeting to lysosomes. *J Cell Sci.*
739 115:185-194.

740 Ogata, S., and M. Fukuda. 1994. Lysosomal targeting of Limp II membrane glycoprotein
741 requires a novel Leu-Ile motif at a particular position in its cytoplasmic tail. *J Biol*
742 *Chem.* 269:5210-5217.

743 Ohno, H., M.C. Fournier, G. Poy, and J.S. Bonifacino. 1996. Structural determinants of
744 interaction of tyrosine-based sorting signals with the adaptor medium chains. *J Biol*
745 *Chem.* 271:29009-29015.

746 Ohno, H., J. Stewart, M.C. Fournier, H. Bosshart, I. Rhee, S. Miyatake, T. Saito, A.
747 Gallusser, T. Kirchhausen, and J.S. Bonifacino. 1995. Interaction of tyrosine-based
748 sorting signals with clathrin-associated proteins. *Science*. 269:1872-1875.

749 Owada, M., and E.F. Neufeld. 1982. Is there a mechanism for introducing acid hydrolases
750 into liver lysosomes that is independent of mannose 6-phosphate recognition?
751 Evidence from I-cell disease. *Biochem Biophys Res Commun*. 105:814-820.

752 Patwardhan, A., S. Bardin, S. Miserey-Lenkei, L. Larue, B. Goud, G. Raposo, and C.
753 Delevoe. 2017. Routing of the RAB6 secretory pathway towards the lysosome
754 related organelle of melanocytes. *Nat Commun*. 8:15835.

755 Paul-Gilloteaux, P., X. Heiligenstein, M. Belle, M.C. Domart, B. Larjani, L. Collinson, G.
756 Raposo, and J. Salamero. 2017. eC-CLEM: flexible multidimensional registration
757 software for correlative microscopies. *Nat Methods*. 14:102-103.

758 Peden, A.A., V. Oorschot, B.A. Hesser, C.D. Austin, R.H. Scheller, and J. Klumperman.
759 2004. Localization of the AP-3 adaptor complex defines a novel endosomal exit site
760 for lysosomal membrane proteins. *J Cell Biol*. 164:1065-1076.

761 Pereira, C., D. Stalder, G.S.F. Anderson, A.S. Shun-Shion, J. Houghton, R. Antrobus, M.A.
762 Chapman, D.J. Fazakerley, and D.C. Gershlick. 2023. The exocyst complex is an
763 essential component of the mammalian constitutive secretory pathway. *J Cell Biol*.
764 222.

765 Pols, M.S., E. van Meel, V. Oorschot, C. ten Brink, M. Fukuda, M.G. Swetha, S. Mayor, and
766 J. Klumperman. 2013. hVps41 and VAMP7 function in direct TGN to late endosome
767 transport of lysosomal membrane proteins. *Nat Commun*. 4:1361.

768 Puertollano, R., R.C. Aguilar, I. Gorshkova, R.J. Crouch, and J.S. Bonifacino. 2001. Sorting
769 of mannose 6-phosphate receptors mediated by the GGAs. *Science*. 292:1712-1716.

770 Rabouille, C. 2017. Pathways of Unconventional Protein Secretion. *Trends Cell Biol*. 27:230-
771 240.

772 Reczek, D., M. Schwake, J. Schroder, H. Hughes, J. Blanz, X. Jin, W. Brondyk, S. Van
773 Patten, T. Edmunds, and P. Saftig. 2007. LIMP-2 is a receptor for lysosomal
774 mannose-6-phosphate-independent targeting of beta-glucocerebrosidase. *Cell*.
775 131:770-783.

776 Robinson, M.S. 2004. Adaptable adaptors for coated vesicles. *Trends Cell Biol*. 14:167-174.

777 Robinson, M.S., D.A. Sahlender, and S.D. Foster. 2010. Rapid inactivation of proteins by
778 rapamycin-induced rerouting to mitochondria. *Dev Cell*. 18:324-331.

779 Sandoval, I.V., and O. Bakke. 1994. Targeting of membrane proteins to endosomes and
780 lysosomes. *Trends Cell Biol*. 4:292-297.

781 Sandoval, I.V., S. Martinez-Arca, J. Valdeuza, S. Palacios, and G.D. Holman. 2000. Distinct
782 reading of different structural determinants modulates the dileucine-mediated
783 transport steps of the lysosomal membrane protein LIMP II and the insulin-sensitive
784 glucose transporter GLUT4. *J Biol Chem*. 275:39874-39885.

785 Schindelin, J., I. Arganda-Carreras, E. Frise, V. Kaynig, M. Longair, T. Pietzsch, S.
786 Preibisch, C. Rueden, S. Saalfeld, B. Schmid, J.Y. Tinevez, D.J. White, V.
787 Hartenstein, K. Eliceiri, P. Tomancak, and A. Cardona. 2012. Fiji: an open-source
788 platform for biological-image analysis. *Nat Methods*. 9:676-682.

789 Slot, J.W., and H.J. Geuze. 1985. A new method of preparing gold probes for multiple-
790 labeling cytochemistry. *Eur J Cell Biol*. 38:87-93.

791 Slot, J.W., H.J. Geuze, S. Gigengack, G.E. Lienhard, and D.E. James. 1991. Immuno-
792 localization of the insulin regulatable glucose transporter in brown adipose tissue of
793 the rat. *J Cell Biol*. 113:123-135.

794 Stockli, J., S. Honing, and J. Rohrer. 2004. The acidic cluster of the CK2 site of the cation-
795 dependent mannose 6-phosphate receptor (CD-MPR) but not its phosphorylation is
796 required for GGA1 and AP-1 binding. *J Biol Chem*. 279:23542-23549.

797 Tabuchi, N., K. Akasaki, and H. Tsuji. 2000. Two acidic amino acid residues, Asp(470) and
798 Glu(471), contained in the carboxyl cytoplasmic tail of a major lysosomal membrane
799 protein, LGP85/LIMP II, are important for its accumulation in secondary lysosomes.
800 *Biochem Biophys Res Commun*. 270:557-563.

801 Vega, M.A., F. Rodriguez, B. Segui, C. Cales, J. Alcalde, and I.V. Sandoval. 1991. Targeting
802 of lysosomal integral membrane protein LIMP II. The tyrosine-lacking carboxyl
803 cytoplasmic tail of LIMP II is sufficient for direct targeting to lysosomes. *J Biol Chem.*
804 266:16269-16272.

805 Waheed, A., S. Gottschalk, A. Hille, C. Krentler, R. Pohlmann, T. Bräulke, H. Hauser, H.
806 Geuze, and K. von Figura. 1988. Human lysosomal acid phosphatase is transported
807 as a transmembrane protein to lysosomes in transfected baby hamster kidney cells.
808 *EMBO J.* 7:2351-2358.

809 White, J., L. Johannes, F. Mallard, A. Girod, S. Grill, S. Reinsch, P. Keller, B. Tzschaschel,
810 A. Echard, B. Goud, and E.H. Stelzer. 1999. Rab6 coordinates a novel Golgi to ER
811 retrograde transport pathway in live cells. *J Cell Biol.* 147:743-760.

812 Williams, M.A., and M. Fukuda. 1990. Accumulation of membrane glycoproteins in
813 lysosomes requires a tyrosine residue at a particular position in the cytoplasmic tail. *J*
814 *Cell Biol.* 111:955-966.

815 Zachos, C., J. Blanz, P. Saftig, and M. Schwake. 2012. A critical histidine residue within
816 LIMP-2 mediates pH sensitive binding to its ligand beta-glucocerebrosidase. *Traffic.*
817 13:1113-1123.

818 Zhao, Y., J. Ren, S. Padilla-Parra, E.E. Fry, and D.I. Stuart. 2014. Lysosome sorting of beta-
819 glucocerebrosidase by LIMP-2 is targeted by the mannose 6-phosphate receptor. *Nat*
820 *Commun.* 5:4321.

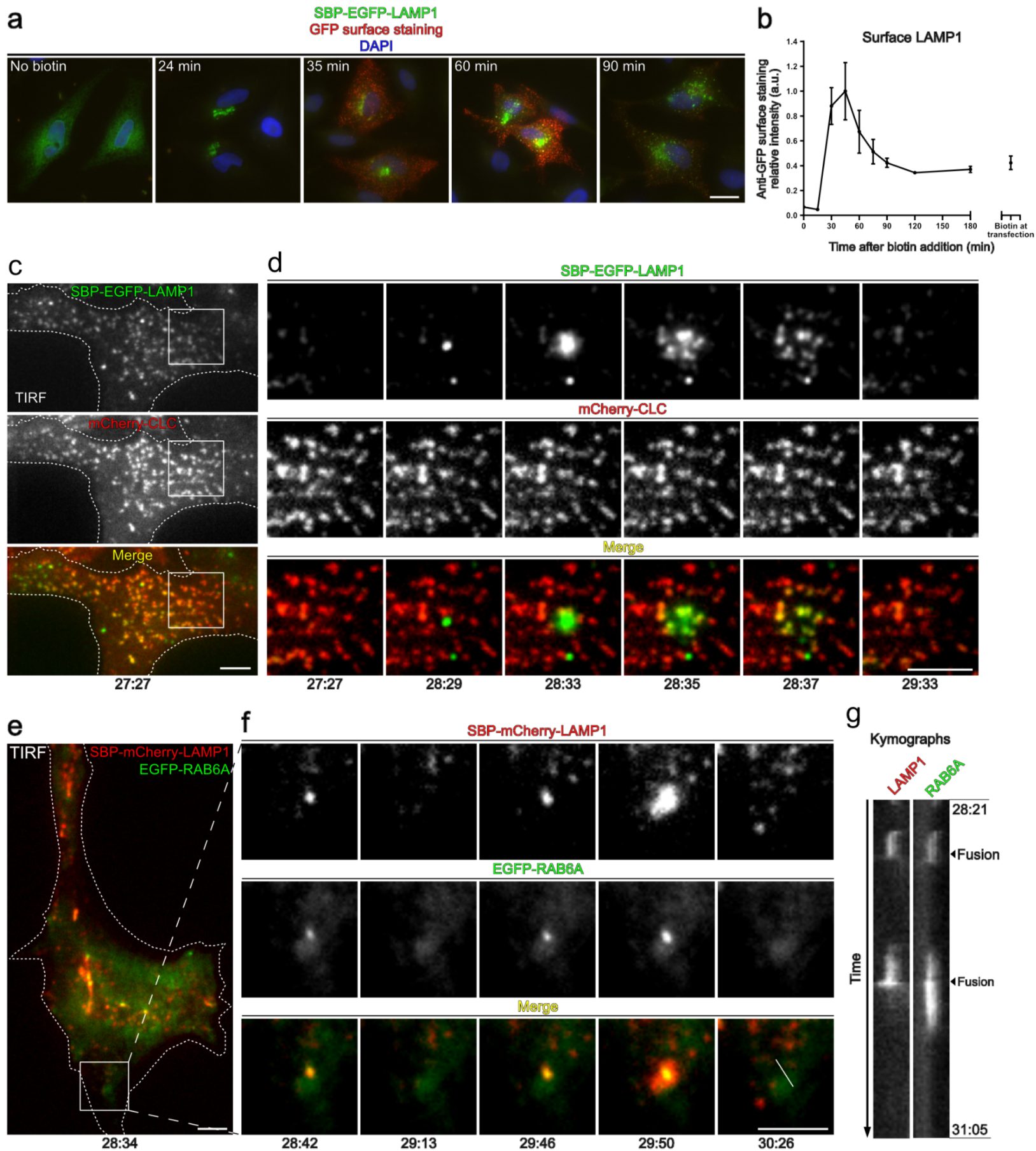
821 Zhu, Y., B. Doray, A. Poussu, V.P. Lehto, and S. Kornfeld. 2001. Binding of GGA2 to the
822 lysosomal enzyme sorting motif of the mannose 6-phosphate receptor. *Science.*
823 292:1716-1718.

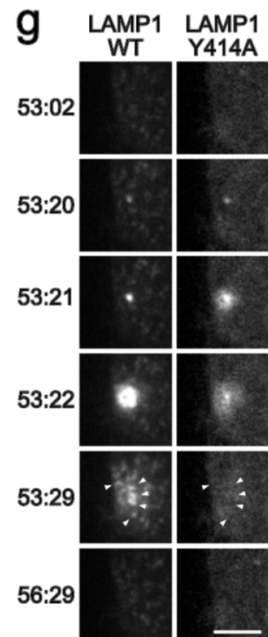
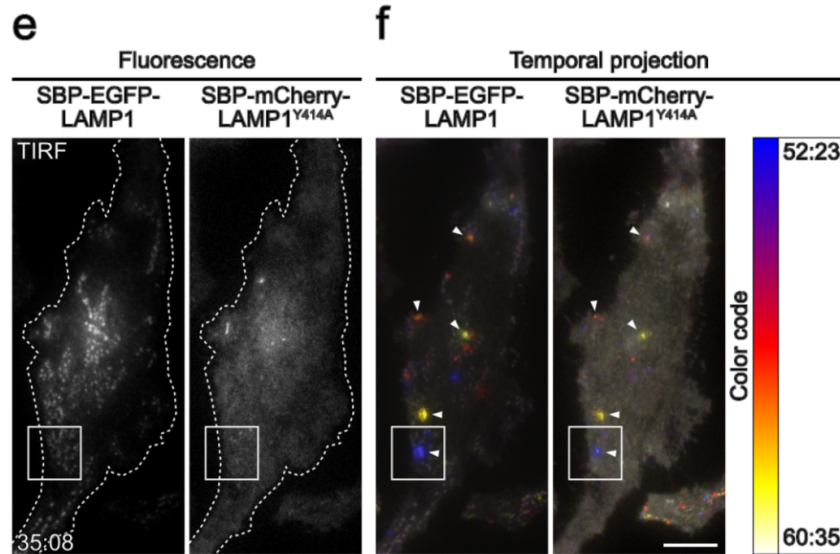
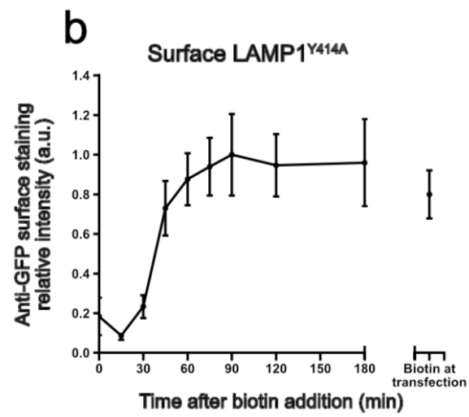
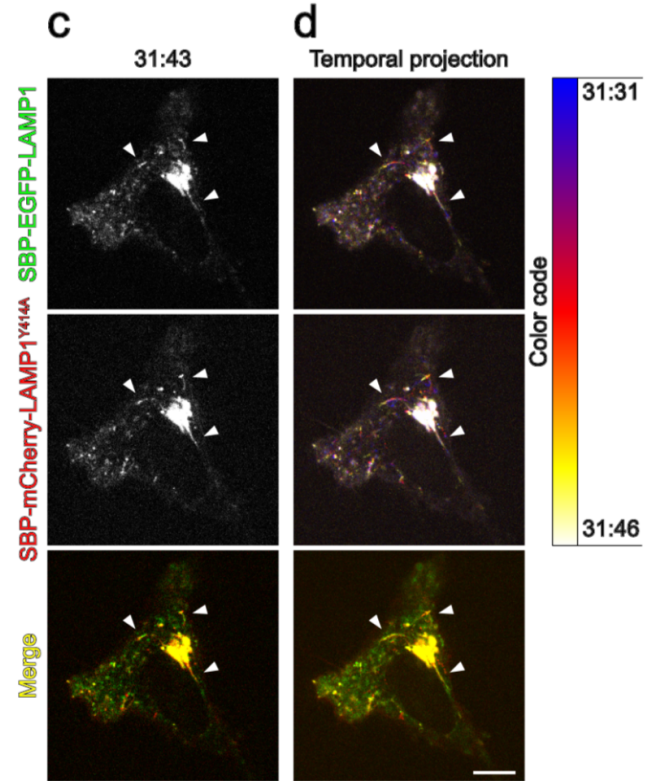
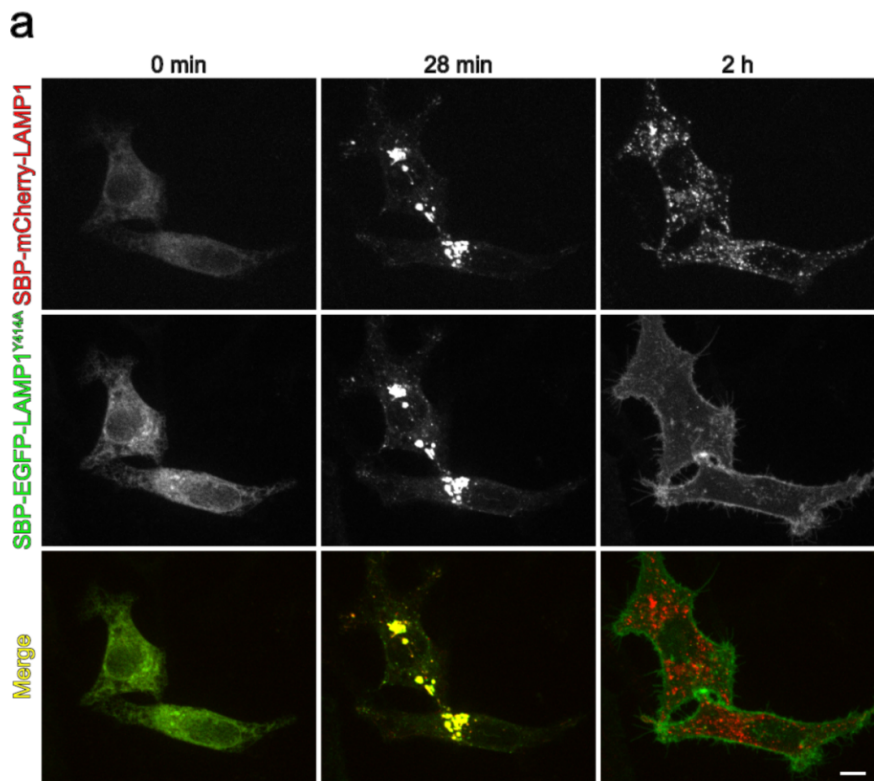
824

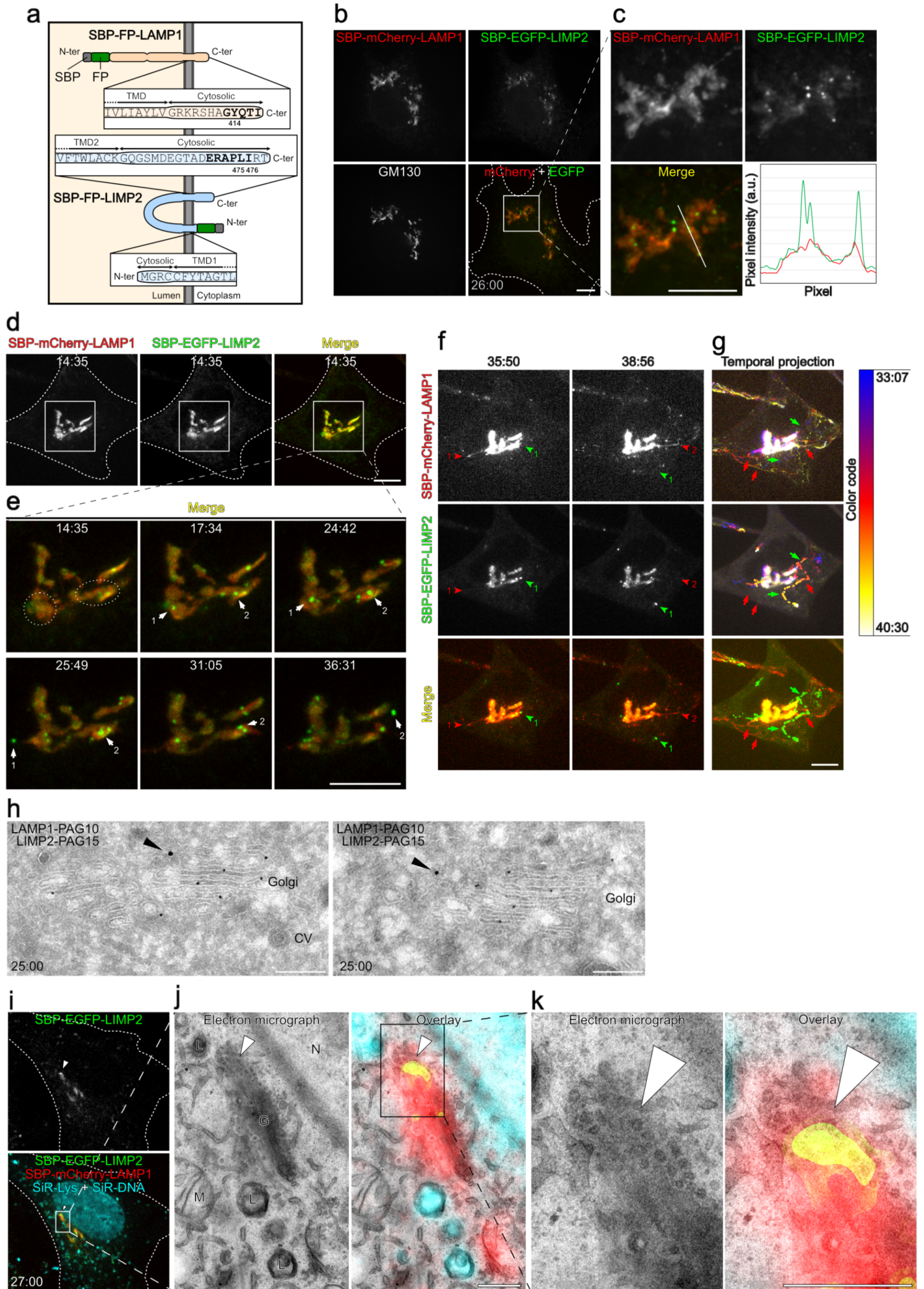
825

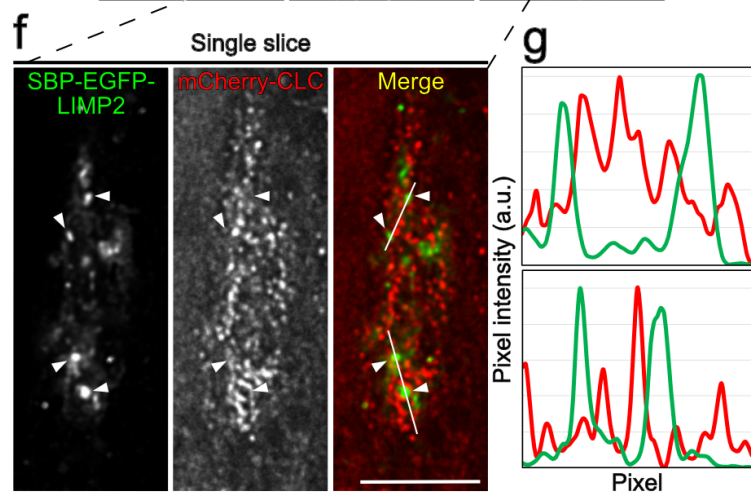
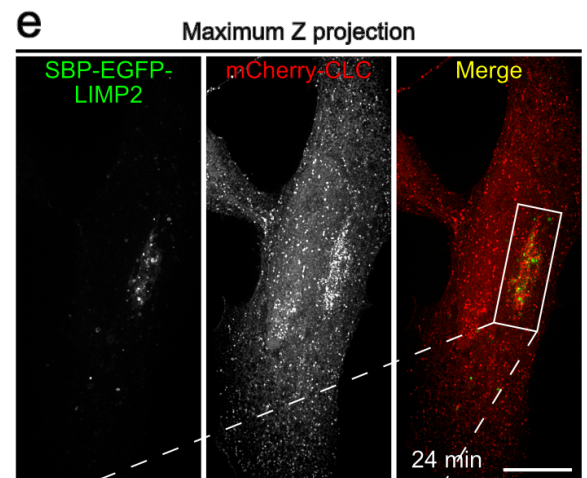
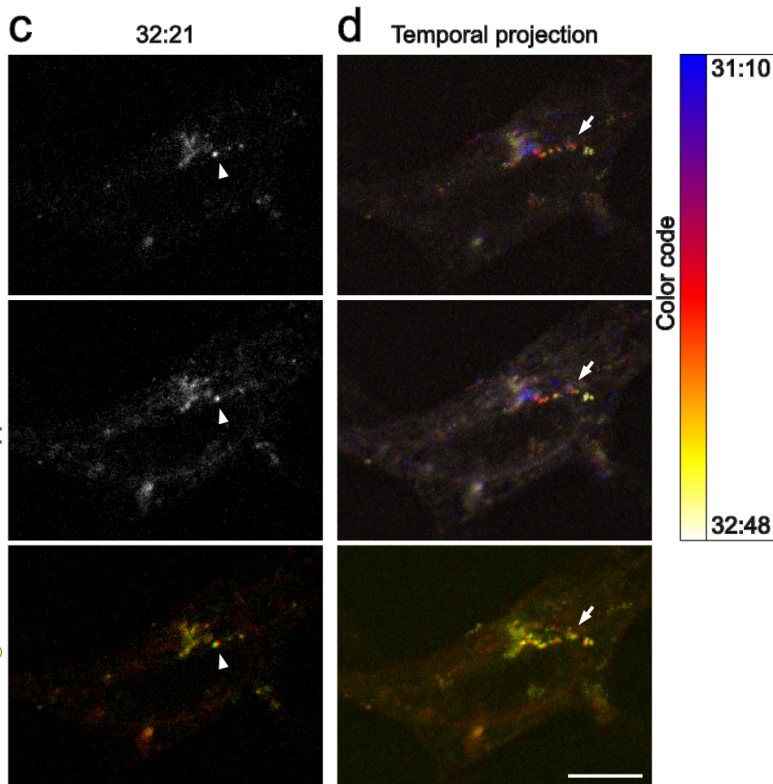
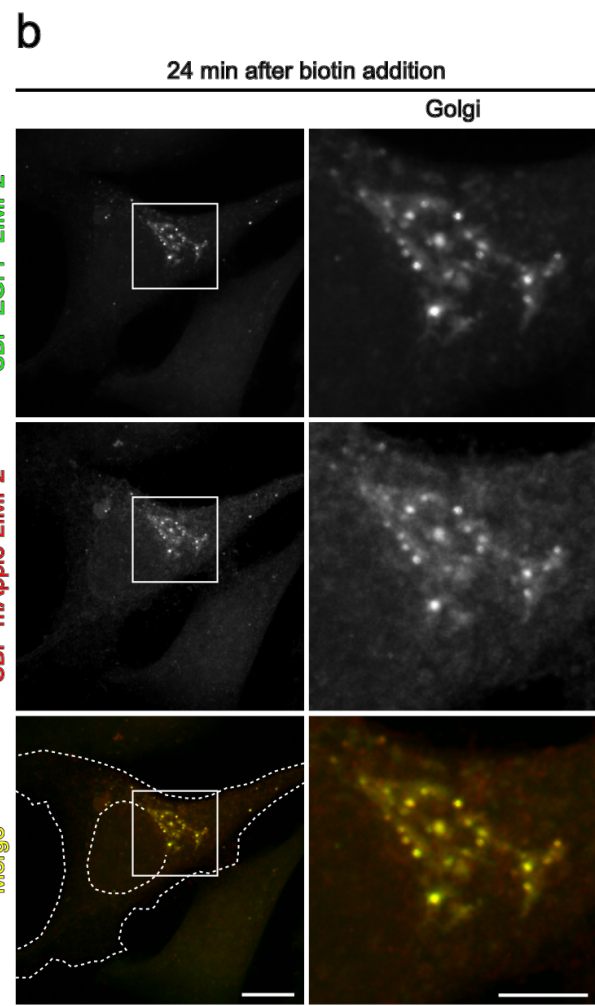
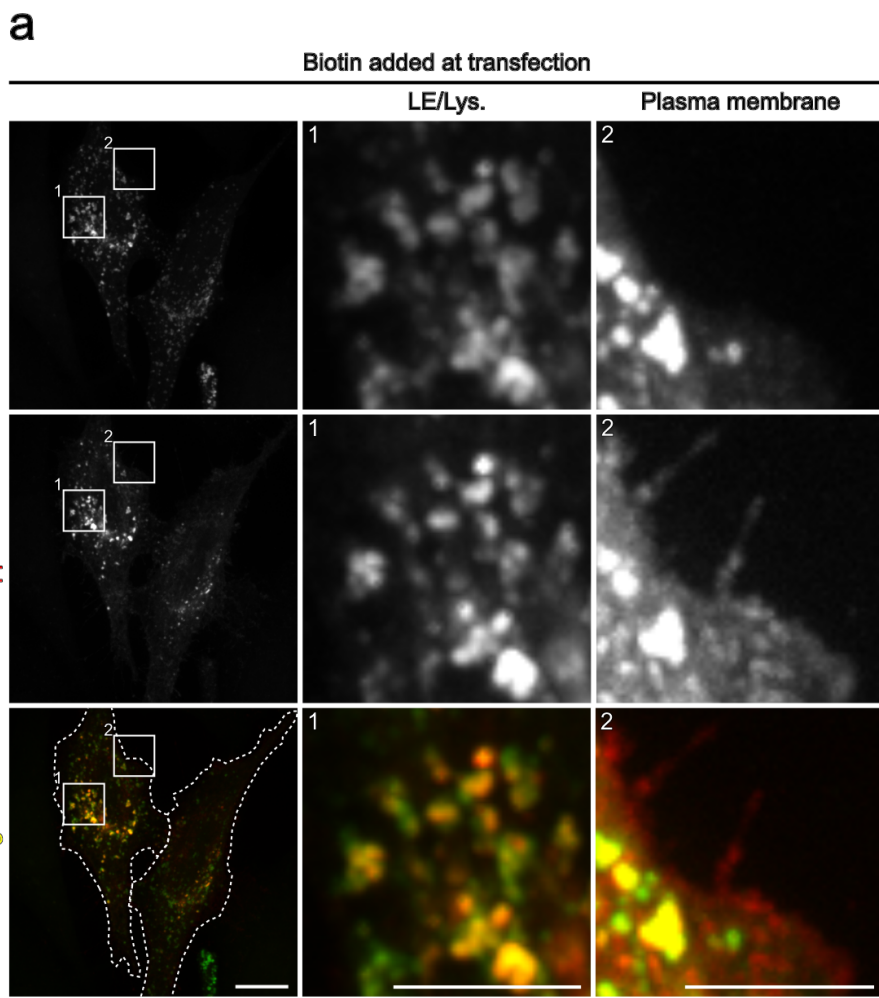
826

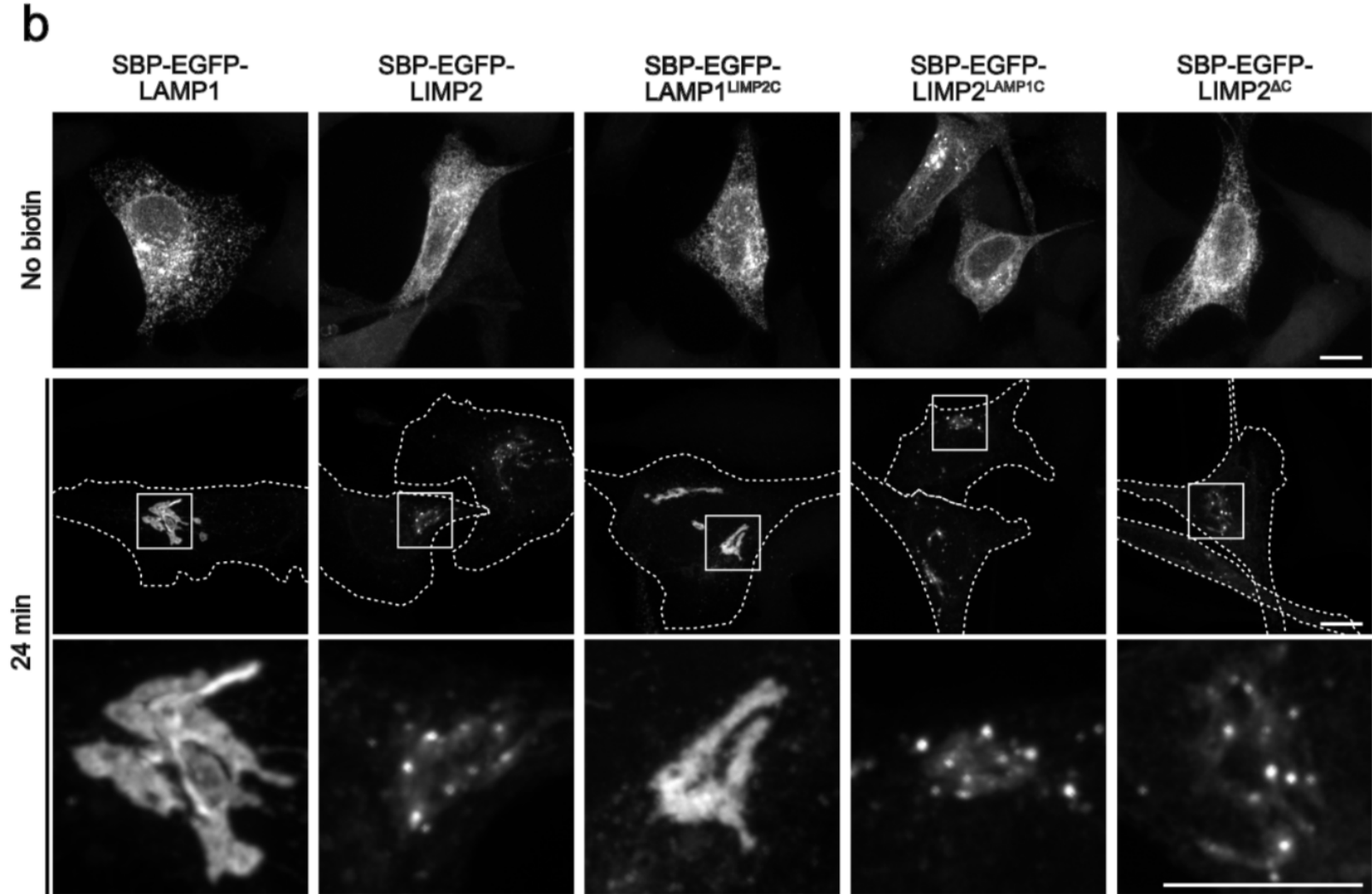
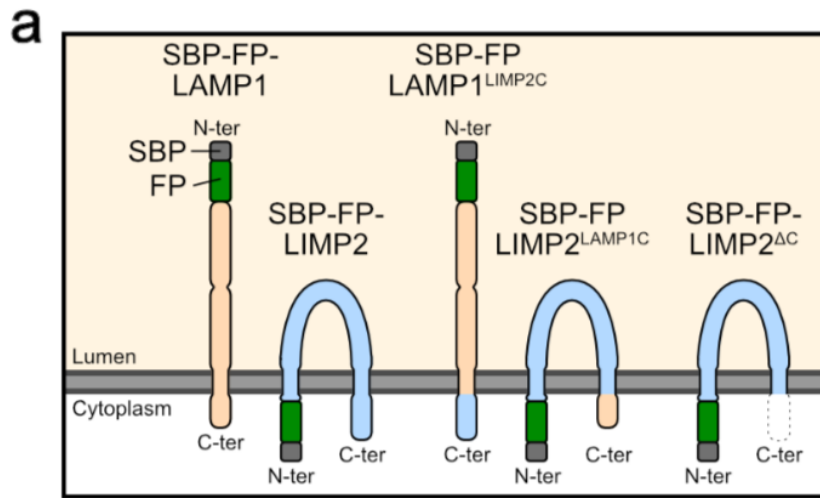
827











828
829
830
831
832
833
834
835
836
837
838
839
840
841
842
843
844
845
846
847

Figure 1. RUSH-synchronised LAMP1 is transported from the Golgi apparatus to the cell surface before being internalized from clathrin-coated pits.

(a) Widefield microscopy images of HeLa cells transiently expressing SBP-EGFP-LAMP1 and Streptavidin-KDEL. Cells were incubated with biotin for the indicated times, stained with an anti-GFP antibody without permeabilization. Scale bar: 5 μ m. (b) Flow cytometry measurement of the surface anti-GFP surface signal intensity of cells treated as in (a). Median anti-GFP intensity of GFP-positive cells normalised to the maximum value is shown. n = 3 independent experiments. Error bars: SEM. (c-d) TIRF images of living HeLa cells transiently expressing SBP-EGFP-LAMP1, Streptavidin-KDEL and mCherry-clathrin light chain (CLC) acquired at the indicated times after the addition of biotin. Scale bars: 5 μ m. (d) Enlargement of the boxed area depicted in (c). (e) Time-lapse acquisition of a fusion event magnified from the boxed region in (c). (e-f) TIRF images of living HeLa cells transiently expressing SBP-mCherry-LAMP1, Streptavidin-KDEL and EGFP-RAB6A. Scale bars: 5 μ m. (f) Fusion events magnified from the boxed region in (e). (g) Kymographs along the line in (f) between the two indicated times. Dotted lines highlight the cell contour. Time in min:s.

848
849
850
851
852
853
854
855
856
857
858
859
860
861
862
863
864
865
866
867
868
869
870

Figure 2. LAMP1^{Y414A} is blocked at the cell surface but follows the same Golgi-to-plasma membrane route as LAMP1 wild-type.

(a) Living HeLa cells transiently expressing both SBP-mCherry-LAMP1 (WT) and SBP-EGFP-LAMP1^{Y414A} and Streptavidin-KDEL. The same cells were imaged at different times after the addition of biotin. Images correspond to maximum Z projections of several slices acquired with a spinning disk microscope. Scale bar: 10 μ m. (b) Flow cytometry quantification of the presence of SBP-EGFP-LAMP1^{Y414A} at the plasma membrane. HeLa cells transiently expressing SBP-EGFP-LAMP1^{Y414A} and Streptavidin-KDEL were incubated with biotin for different times, stained with an anti-GFP antibody without permeabilization. Median anti-GFP intensity of GFP-positive cells normalised to the maximum value is shown. n = 3 independent experiments. Error bars: SEM. (c-d) Living HeLa cells transiently expressing both SBP-EGFP-LAMP1 and SBP-mCherry-LAMP1^{Y414A} and Streptavidin-KDEL were acquired every second. Scale bar: 10 μ m. (c) Single Z-slice acquired with a spinning-disk microscope at the indicated time after biotin addition. Arrowheads indicate Golgi exit events. (d) Color-coded temporal projections between the two indicated times. (e-f) TIRF images of living HeLa cells transfected as in (c) and acquired every second. Scale bar: 10 μ m. (f) Color-coded temporal projections between the indicated times. Arrowheads indicate fusion events with the plasma membrane. (g) Magnified view of boxed areas in (e-f). Arrowheads indicate the retention of LAMP1 retention points in clathrin-coated pits. Scale bar: 5 μ m. Time in min:s.

871

872 **Figure 3. LAMP1 and LIMP2 are segregated and sorted at the Golgi apparatus.**

873 (a) Schematic representations of LAMP1 and LIMP2 topologies, tagging and
874 cytosolic motifs. Clathrin adaptors recruitment signals are shown in bold. FP:
875 fluorescent protein. (b-c) High-resolution images of HeLa cells transiently transfected
876 to express Streptavidin-KDEL, SBP-mCherry-LAMP1, Streptavidin-HA-Endo-KKXX
877 and SBP-EGFP-LIMP2. Cells were incubated with biotin for 26 min, fixed and stained
878 for GM130. The images correspond to maximum Z projection of high-resolution image
879 stacks. Scale bars: 10 μ m. (c) Magnified view of the boxed area in b. Linescan of pixel
880 intensities along the line normalised on the Golgi mean intensity. (d-g) Living HeLa
881 cells transfected to express Streptavidin-KDEL, SBP-mCherry-LAMP1, mini-li-
882 Streptavidin and SBP-EGFP-LIMP2 acquired every two seconds. Images correspond
883 to maximum Z projection of spinning-disk stacks acquired at indicated times after biotin
884 addition. Scale bars: 10 μ m. (e) Magnified view of the boxed area in d. Arrows track
885 two puncta from their appearance to their Golgi exit. The dotted ovals highlight the
886 appearance area of the two tracked puncta. (f) Same cells as in d-e. Red and green
887 arrowheads indicate carriers that exit the Golgi apparatus for SBP-mCherry-LAMP1
888 and SBP-EGFP-LIMP2, respectively. (g) Color-coded temporal projection between the
889 two indicated times. Arrows track the carriers leaving the Golgi apparatus. Scale bar:
890 10 μ m. (h) Cryo-immuno electron microscopy pictures of HeLa cells transiently
891 expressing Streptavidin-KDEL, SBP-mCherry-LAMP1, Streptavidin-HA-Endo-KKXX
892 and SBP-EGFP-LIMP2. Cells were incubated with biotin for 25 min, fixed and prepared
893 for cryo-immuno electron microscopy. SBP-mCherry-LAMP1 was detected with an
894 anti-mCherry antibody and 10 nm-gold particles conjugated to Protein A (PAG10).
895 SBP-EGFP-LIMP2 was detected with an anti-GFP antibody and 15 nm-gold particles
896 conjugated to Protein A (PAG15). Arrowheads highlight SBP-EGFP-LIMP2; CV:
897 coated vesicle. Scale bar: 250 nm (i-k) Correlative light-electron microscopy of SBP-
898 EGFP-LIMP2 and SBP-mCherry-LAMP1. HeLa cells were transfected like in b and c
899 and were live stained using SiR-lysosome (SiR-Lys) and SiR-DNA, incubated with
900 biotin for 27 min, fixed, acquired for fluorescence, and then prepared for transmission
901 electron microscopy (TEM). The arrowhead indicates a SBP-EGFP-LIMP2 bright
902 punctum at the Golgi apparatus. (i) Images are confocal spinning-disk Z slices. Scale
903 bar: 10 μ m. (j,k) TEM images and fluorescence-EM correlation. The SiR-lysosome
904 staining was used for the correlation. L, lysosome; M, mitochondria; N, nucleus; G,
905 Golgi stack. Scale bar: 1 μ m. Time in min:s.

906

907

908 **Figure 4. LIMP2 [D/E]XXXL[L/I] motif is not involved in its sorting at the Golgi**
909 **apparatus.**

910 (a-b) HeLa cells transiently expressing mini-li-Streptavidin, SBP-EGFP-LIMP2 WT,
911 streptavidin-HA-Endo-KKXX and SBP-mApple-LIMP2^{AA}. Images correspond to
912 maximum Z projection of spinning disk confocal stacks. Scale bars: 10 μ m, magnified
913 views: 5 μ m. Cells were fixed 24 h after transfection. (b) Cells were incubated with

914 biotin for 24 min and fixed. **(c-d)** HeLa cells were transfected to express mini-li-
915 Streptavidin, SBP-EGFP-LIMP2 WT and SBP-mApple-LIMP2^{AA}. Pictures were
916 acquired every two seconds to follow the Golgi exit events. Scale bar: 10 μ m. **(c)**
917 Arrowheads point out a compartment exiting the Golgi apparatus. **(d)** Color-coded
918 temporal projection between the two indicated times. Arrows indicate a track exiting
919 the Golgi apparatus. **(e-f)** High resolution image of HeLa cells transiently expressing
920 mini-li-Streptavidin, SBP-EGFP-LIMP2 and mCherry-clathrin light chain (CLC). The
921 cells were incubated with biotin for 24 min and fixed. Images correspond to maximum
922 Z projections **(e)** or single slices **(f)** of high-resolution image stacks and deconvolved.
923 **(e)** Scale bar: 10 μ m. **(f)** Arrowheads indicate LIMP2 bright puncta at the Golgi
924 apparatus. Scale bar: 5 μ m. **(g)** Linescans of pixel intensity along the two lines in **(f)**,
925 normalised to the maxima. Time in min:s.

926
927

928 **Figure 5. LIMP2 C-terminal cytosolic domain is not involved in its sorting at**
929 **the Golgi apparatus.**

930 **(a)** Schematic representation of the LAMP1/LIMP2 chimeras and LIMP2 deletion
931 mutant. **(b)** HeLa cells were transfected to express Streptavidin-KDEL (for SBP-
932 EGFP-LAMP1 or SBP-EGFP-LAMP1^{LIMP2C}) or mini-li-Streptavidin (for SBP-EGFP-
933 LIMP2, SBP-EGFP-LIMP2^{LAMP1C} or SBP-EGFP-LIMP2^{ΔC} treated or not with biotin for
934 24 min and fixed. Images correspond to maximum Z projection of spinning disk
935 confocal image stacks. Dotted lines indicate cell contour. Bottom panel corresponds
936 to enlargement of the Golgi region boxed in the upper lane. Scale bars: 10 μ m.

937

938

939 **Supplementary figure 1. RUSH-synchronised LAMP1 reaches late**
940 **endosomes/lysosomes.**

941 Widefield microscopy images of HeLa **(a,b)**, SUM159 **(c)** and RPE-1 **(d)** cells
942 expressing SBP-mCherry-LAMP1 and Streptavidin-KDEL. The cells were incubated
943 with biotin for the indicated times, fixed and stained for the ER marker PDI isoform A3,
944 the Golgi marker GM130 or giantin or the LE/lysosome marker LAMTOR4. **(a)** Scale
945 bar: 10 μ m. **(b)** Magnified views of boxed areas. Arrowheads point SBP-mCherry-
946 LAMP1 positive compartments decorated with LAMTOR4. Scale bars: 5 μ m (a,b), 10
947 μ m (c,d). **(e)** Flow cytometry measurement of the surface anti-GFP surface signal
948 intensity of cells treated as in c and d. Median anti-GFP intensity of GFP-positive cells
949 normalised to the maximum value is shown. n = 2 independent experiments. Error
950 bars: SEM.

951

952

953 **Supplementary figure 2. Endogenous LAMP1 transits through the cell surface**
954 **before reaching lysosomes**

955 **(a)** Schematic representation of the editing strategy of the LAMP1 gene. The signal
956 peptide is encoded by a coding sequence located on Exon1 and Exon2 (with intron 1

957 in between). The gRNA aligns downstream of the signal peptide. The dashed black
958 and grey lines represent a break in scale in the LAMP1 gene and protein, respectively.
959 Numbers on the scheme of LAMP1 protein correspond to the position of the first amino
960 acid of each domain. The donor DNA to introduce SBP and mCherry contains two
961 homology arms of 800 bp each. Green arrows correspond to the primers used for the
962 PCR analysis of genomic DNA depicted in b. LAMP1^{EN}: endogenously tagged LAMP1,
963 TMD: transmembrane domain, cyt.: cytoplasmic domain.

964 **(b)** Genomic DNA of the corresponding SUM159 cells was extracted from a clonal
965 population. The presence of the knock-in construct was assessed by PCR using
966 external primers (see a). Size of the bands of the DNA ladder (1kb Plus DNA ladder
967 from ThermoFisher Scientific) is expressed in base pairs. The expected size of the
968 PCR fragment from the wild-type locus (non-edited) was 2298 bp and from the edited
969 locus containing the SBP-mCherry insertion was 3138 bp. Str-KDEL: overexpression
970 of the RUSH ER hook Streptavidin-KDEL introduced by lentiviral transduction.

971 **(c)** The homozygote clone with knock-in of SBP-mCherry in LAMP1 locus and
972 overexpressing the ER hook Str-KDEL was either non treated or incubated with biotin
973 for the indicated times. SUM159 wild-type cells were used as a control.
974 Immunostaining with an anti-SBP antibody was used to amplify the fluorescence signal
975 for SBP-mCherry-Lamp1 (upper panels and red on merge pictures). Lysosomes were
976 labelled using an anti-LBPA antibody and DNA was stained with DAPI. Scale bar: 10
977 μ m.

978 **(d)** The presence of SBP-mCherry-LAMP1^{EN} at the cell surface upon trafficking was
979 monitored by flow cytometry. The cells were incubated with biotin for the indicated
980 times and then stained with an anti-SBP antibody without permeabilization. The
981 fluorescence signal was normalised to the maximum value of the series corresponding
982 to the SBP-mCherry-LAMP1^{EN} + Str-KDEL cells. n=3 independent experiments. Error
983 bars correspond to SEM.

984

985 **Supplementary figure 3.** RUSH-synchronised LIMP2, LAMP2 and LAP reach late
986 endosomes/lysosomes.

987 **(a-f)** Widefield microscopy images of HeLa cells transfected to express the mini-li-
988 Streptavidin **(a-b)** or Streptavidin-KDEL **(c-f)** and indicated cargos. The cells were
989 incubated with biotin for the indicated times, fixed and stained for PDI isoform A3 or
990 GM130 and LAMTOR4. **(a, c, e)** Scale bars: 10 μ m. **(b, d, f)** Magnified views of boxed
991 areas. Arrowheads point out compartments colocalising with LAMTOR4. Scale bars:
992 5 μ m.

993

994 **Supplementary figure 4.** LAMP1 and LAMP2 are not sorted at the Golgi
995 apparatus.

996 **(a-b)** HeLa cells were transfected to express Streptavidin-KDEL, SBP-mCherry-
997 LAMP1 and SBP-EGFP-LAMP2. Cells were incubated with biotin for 26 min and fixed.
998 The images correspond to maximum Z projection of high-resolution images stacks.
999 Scale bars: 10 μ m. **(b)** Magnified view of the boxed area in a. The curves show the
1000 pixel intensities along the white line normalised to the Golgi mean intensity. **(c-d)** The

1001 cells were transfected like in (a-b) and were acquired live. Scale bar: 10 μ m. (c)
1002 Images correspond to maximum Z projection of spinning-disk confocal stacks acquired
1003 at indicated time after biotin addition. The arrowheads point out Golgi exit events. (d)
1004 Color-coded temporal projection between indicated times. Arrowheads point out Golgi
1005 exit tracks. Time in min:s. (e) Flow cytometry measurement of the surface anti-GFP
1006 surface signal intensity of HeLa cells transiently expressing Streptavidin-KDEL and
1007 SBP-EGFP-LAMP2. Median anti-GFP intensity of GFP-positive cells normalised to the
1008 maximum value is shown. n = 2 independent experiments. Error bars: SEM.

1009

1010 **Supplementary figure 5.** LAMP1 and LAP are not sorted at the Golgi apparatus.

1011 (a-b) HeLa cells were transfected to express Streptavidin-KDEL, SBP-EGFP-
1012 LAMP1 and SBP-mCherry-LAP. Cells were incubated with biotin for 26 min and fixed.
1013 The images are maximum Z projection of high-resolution images stacks. Scale bars:
1014 10 μ m. (b) Magnified view of the boxed area in (a). Linescan of pixel intensity along
1015 the line normalised to the Golgi mean intensity. (c-d) The cells were transfected like
1016 in (a-b). Scale bar: 10 μ m. (c) Images are maximum Z projection of spinning-disk
1017 confocal stacks acquired at indicated time after biotin addition. The arrowheads point
1018 out Golgi exit events. (d) Color-coded temporal projection between indicated times.
1019 Arrowheads point out Golgi exit tracks. Time in min:s. (e) Flow cytometry
1020 measurement of the surface anti-GFP surface signal intensity of HeLa cells transiently
1021 expressing Streptavidin-KDEL and SBP-EGFP-LAP. Median anti-GFP intensity of
1022 GFP-positive cells normalised to the maximum value is shown. n = 2 independent
1023 experiments. Error bars: SEM.

1024

1025 **Supplementary figure 6.** LAMP1 and LIMP2 are segregated in the Golgi apparatus
1026 in SUM159 and RPE-1 cells.

1027 (a) SUM159 cells transiently transfected to express Streptavidin-KDEL, SBP-
1028 mCherry-LAMP1, Streptavidin-HA-Endo-KKXX and SBP-EGFP-LIMP2. The pictures
1029 displayed correspond to a maximum intensity projection of spinning disk Z-slices of
1030 cells incubated with biotin for 60 min.

1031 (b) RPE-1 cells transiently transfected to express Streptavidin-KDEL, SBP-mCherry-
1032 LAMP1, Mini-li-Streptavidin-HA and SBP-EGFP-LIMP2. The pictures displayed
1033 correspond to a maximum intensity projection of spinning disk Z-slices of cells
1034 incubated with biotin for 16 min.

1035 Scale bars: 10 μ m

1036

1037 **Supplementary figure 7.** LIMP2 [D/E]XXXL[L/I] motif is not involved in the
1038 formation of LIMP2 bright puncta at the Golgi apparatus.

1039 (a-b) HeLa cells transiently expressing mini-li-Streptavidin and SBP-EGFP-LIMP2
1040 (a) or SBP-LIMP2-LIMP2^{AA} (b). Biotin was added at the time of transfection. The cells
1041 were fixed the day after and stained with anti-LAMTOR4 and HCS CellMask. Images
1042 are maximum projection of confocal Z stacks. Scale bars: 10 μ m, magnified views: 5
1043 μ m. (c-d) HeLa cells were transfected like in (a-b). The day after transfection, cells

1044 were incubated with biotin for 24 min, fixed and stained for GM130. Images are
1045 maximum projections of confocal Z stacks. Scale bars: 10 μm , magnified views: 5 μm .
1046
1047